8/18 27/9-2-83 Mc ①

Dr. 1719-1

SANDIA REPORT

SAND82—1315 • Unlimited Release • UC—70

Printed August 1983

I-10982

Analysis of Rock Mechanics Properties of Volcanic Tuff Units from Yucca Mountain, Nevada Test Site

SAND--82-1315

DE83 017056

Ronald H. Price

Prepared by
Sandia National Laboratories
Albuquerque, New Mexico 87185 and Livermore, California 94550
for the United States Department of Energy
under Contract DE-AC04-76DP00789

MASTER

SF 2900-Q(6-82)

DISTRIBUTION OF THIS DOCUMENT IS UNLIMITED

DISCLAIMER

Issued by Sandia National Laboratories, operated for the United States Department of Energy by Sandia Corporation.

Printed in the United States of America
Available from
National Technical Information Service
U.S. Department of Commerce
5285 Port Royal Road
Springfield, VA 22161

NTIS price codes
Printed copy: A05
Microfiche copy: A01

Distribution
Category UC-70

SAND82-1315
Unlimited Release
Printed August 1983

Analysis of the Rock Mechanics Properties of Volcanic Tuff Units from Yucca Mountain, Nevada Test Site

R. H. Price
Geomechanics Division 1542
Sandia National Laboratories
Albuquerque, New Mexico 87185

ABSTRACT

Over two hundred fifty mechanical experiments have been run on samples of tuff from Yucca Mountain, Nevada Test Site. Cores from the Topopah Spring, Calico Hills, Bullfrog and Tram tuff units were deformed to collect data for an initial evaluation of mechanical (elastic and strength) properties of the potential horizons for emplacement of commercial nuclear wastes. The experimental conditions ranged in sample saturation from room dry to fully saturated, confining pressure from 0.1 to 20 MPa, pore pressure from 0.1 to 5 MPa, temperature from 23 to 200°C, and strain rate from 10^{-7} to 10^{-2} s^{-1}. These test data have been analyzed for variations in elastic and strength properties with changes in test conditions, and to study the effects of bulk-rock characteristics on mechanical properties. In addition to the site-specific data on Yucca Mountain tuff, mechanical test results on silicic tuff from Rainier Mesa, Nevada Test Site, are also discussed. These data both overlap and augment the Yucca Mountain tuff data, allowing more definitive conclusions to be reached, as well as providing data at some test conditions not covered by the site-specific tests.

Contents

Tables

Figures

Introduction

Yucca Mountain (YM), near the southwest margin of the Nevada Test Site (NTS) in southern Nevada, is being evaluated as a potential site for underground storage of nuclear wastes. Yucca Mountain primarily consists of layered volcanic tuff [8]. Samples from four stratigraphic units have been tested for physical, thermal and mechanical properties as part of the Nevada Nuclear Waste Storage Investigations (NNWSI) Project, administered by the Nevada Operations Office of the U. S. Department of Energy. The four units, in order of decreasing stratigraphic position (increasing depth and age), are as follows: 1. Topopah Spring Member of the Paintbrush Tuff (Tpt), 2. Tuffaceous beds of Calico Hills (Tc), 3. Bullfrog Member of the Crater Flat Tuff (Tcfb), and 4. Tram Member of the Crater Flat Tuff (Tcft). A complete stratigraphic column for Yucca Mountain at drill hole USW G-1 is shown in Figure 1.

Four data reports have presented mechanical data from samples of Topopah Spring [16], Calico Hills [15], Bullfrog [13], and Tram [14] tuffs. In addition to these test series, other mechanical experiments have also been reported [1,8,9,10,18,20] on samples from Yucca Mountain. A compilation of all compressional test conditions and results from the above referenced reports is contained in Appendix 1. All of the above data will be discussed in this report in order to summarize the present state of knowledge of the mechanical properties of tuffs from Yucca Mountain.

Supplementary to the site-specific data, many data have been collected on similar silicic tuff material from Rainier Mesa (RM) at the Nevada Test Site. Olsson and Jones [10] and Wawersik [20] have deformed tuff specimens at various water contents, temperatures and rates. These data will also be analyzed here.

All symbols and abbreviations used in this report can be found in Tables 1 and 2. Within these tables the terms are defined, conventions explained, and standard units assigned.

Test Procedures and Sample Preparation

While all of the above mentioned data will be presented in summary, individual test curves will not be presented. These results, as well as detailed discussions of sample treatment, equipment, experimental procedures and calibrations, are available in the individual data reports.

The large majority of samples tested were right circular cylinders with diameters of 2.54 cm and a length-to-diameter ratio of approximately 2:1. This specimen size allowed the number of test samples to be maximized, since the amount of raw core material was limited in amount and size (approximately 6 cm in diameter). For the large majority of samples, the grain and flaw (pore) sizes were less than one-tenth of the sample diameter; thus, individual grain and pore effects on the bulk mechanical properties were minimized. The 2:1 length-to-diameter ratio reduces end effects (i.e., sample-loading piston interaction), which are much more of a problem at lower ratios, and misalignment (i.e., the production of bending moments), which occurs more frequently when higher ratios are used. Calibrations of force and displacement gages prior to each experimental series have shown that errors in these measurements are in all cases less than three percent. Any major differences in mechanical properties for adjacent tuff samples are, therefore, a result of sample variability (mineralogy, porosity, grain density, etc) or testing procedures. Since the experimental techniques were designed to minimize alignment and other problems, the data scatter is predominantly a result of sample variability.

Elastic Properties

Young's modulus and Poisson's ratio data have been collected in several experimental studies [8,9,10,13,14,15,16,18,20] on tuffs from Yucca Mountain. A statistical analysis [17] of these elastic constants as a function of effective porosity, grain density and zeolitization has been done on unconfined test data using samples of Calico Hills, Bullfrog and Tram tuffs [8,13,14,15,18]. All of the mechanical experiments were run on fully saturated samples at atmospheric pressure (i.e., unconfined), room temperature (23°C) and a 10^{-5} s^{-1} nominal strain rate. The data were fit by the following models:

$$\text{MODEL 1}: \ \text{Log}\, Y = B_0 + B_1 \,\text{Log}\, X$$

$$\text{MODEL 2}: \ \text{Log}\, Y = B_0 + B_1 \,\text{Log}\, X_1 + B_2 \,\text{Log}\, X_2,$$

where Log is a common logarithm to the base 10; X is effective porosity or grain density; X_1 is effective porosity; X_2 is grain density; Y is Young's modulus or Poisson's ratio; and B_0, B_1, B_2 are fitting parameters.

The results of the analysis are summarized in Tables 3 and 4. Six sets of fitting parameters are given by combining the results obtained from tests performed at Sandia National Laboratories - Albuquerque (SNLA) [8,13,14,15] and Terra Tek Inc. (TT) [18] together with three data sets: A. all tuff data, B. zeolitized tuff (i.e., $\rho_g \leq 2.52$ Mg/m^3) data and C. non-zeolitized tuff (i.e., $\rho_g > 2.52$ Mg/m^3) data. Only the statistically significant fits (i.e., an $\alpha \leq .05$) of the model to the data have been listed.

Using grain density as the basis for dividing the tuffs into zeolitized and non-zeolitized is not a rigorous, unique criteria. This material property was chosen since zeolites (hydrous silicates) tend to lower the average grain density of a silicic tuff. Furthermore, all of the test samples (considered in this statistical analysis) with a zeolite content of greater than 5 percent (by weight) were found to have grain densities of less than 2.52 Mg/m^3.

The fits were calculated using an effective porosity equal to the volume of clay (montmorillonite) material in addition to the actual porosity. This action was taken after careful analysis of the data in an effort to increase confidence in the predictive capability of the models. Since clay is a relatively weak, compliant material, considering its volume in an effective porosity is deemed appropriate.

A statistical comparison [17] of the SNLA data and the TT data has been performed due to major differences in the calculated fitting parameters from the two data sets. These results are summarized in Table 5. The average differences for paired data (i.e., data from samples at the same depth) are given, with a positive difference indicating higher SNLA data values. The two labs are beginning discussions of possible explanations for the differences; however, since the reasons are not clear at this time, the results from analyses of each of the data sets are presented, but only the SNLA results will be discussed here.

Statistically, Young's modulus is significantly fit by using both effective porosity and grain density (Model 2) with all of the data. This result does not appear to have any real significance, however, since the fitting constant for grain density (B_2) is negative. Intuitively, this is not realistic because grain density should be directly related to Young's modulus. This is shown by the Model 1 fit of Young's modulus to grain density, and also graphically in Figure 2, with a general trend of increasing Young's modulus with grain density. As a result, the fits of all data to effective porosity (Figure 3) or of a split of the data, on the basis of zeolitization, fit to effective porosity (Figures 4A and 4B) appear to be the best predictive tools available.

Poisson's ratio appears graphically to be neither related to effective porosity (Figure 5), nor to grain density (Figure 6). A statistically significant fit was made, however, to Model 2 with both bulk-rock properties.

Unconfined Strength

Ultimate stress values have been determined for tuff samples from Yucca Mountain under a wide range of experimental conditions [1,8,9,10,13,14,15,16,18,20]. There is a broad data base of unconfined compressive test results which has allowed a statistical analysis to be run on the fit of strength to bulk-rock properties with a power-law model. The only tensile data available are from Brazilian (indirect-tensile) tests, which have been linearly fit to porosity. These analyses will be discussed in the following subsections.

Compressive Strength

The same sets of unconfined, room temperature, constant strain rate experiments [8,13,14,15,18] analyzed in the elastic properties section were also studied [17] for the effects of effective porosity, grain density and zeolitization on unconfined compressive strength (i.e., C_0). Both the models (1 and 2) and the data sets (A, B and C) are identical to those described in the previous topic. The resultant model parameters are given in Table 6.

As mentioned in the Elastic Properties section, an effective porosity, equal to the matrix porosity plus the volume of clay, is being used. Figures 7 and 8 are log-log plots of ultimate stress (strength) versus porosity and versus effective porosity, respectively. These graphs illustrate the more distinct trend when effective porosity, instead of porosity alone, is used. As a result, effective porosity appears to be a good indicator of strength, especially when the data is divided on the basis of zeolitization (Figures 9A and 9B). The addition of grain density in Model 2 results in unrealistic fits (i.e., a negative B_2 parameter for data set A), in statistically insignificant fits to the model (data set B), or in very minor increases in the indices of determination (data set C). Figure 10 is a log-log plot of strength versus grain density, showing the large data scatter, with an indistinct trend of strength directly proportional to grain density, as would be expected.

Figures 11 and 12 are graphs of axial strain at failure versus effective porosity and versus grain density, respectively. Graphically, ultimate strain appears to be insensitive to these bulk-rock properties.

A statistical comparison [17] of the SNLA and TT data has been performed for the ultimate strength and failure strain values. These results are presented in Table 7. As in Table 5, positive average differences indicate higher SNLA data values.

Tensile Strength

Indirect, Brazilian test, measurements of the tensile strengths of samples from all four Yucca Mountain tuff units have been made at Los Alamos National Laboratory [1]. The relationship between unconfined tensile strength (T_0) and porosity is approximately linear (see Figure 13). This linear relationship can be used for the first-order approximations of tensile strength of any Yucca Mountain tuff sample with determined porosity.

Effects of Water

The effects of water saturation on silicic tuff were initially studied on samples of Grouse Canyon tuff (Tbrg) from Rainier Mesa [10]. A total of eighteen water-saturated and oven-dried samples of Grouse Canyon welded tuff were deformed at atmospheric pressure; room temperature; and nominal strain rates of 10^{-6}, 10^{-4} and 10^{-2} s^{-1}. Results are tabulated in Table 8 and graphically presented in Figure 14. The data revealed, at each strain rate, saturated specimen strengths were an average of 30% lower than the corresponding dry sample strengths. As explained by Olsson and Jones [10] : "The fact that the trend lines drawn through the data are parallel suggests that the water effect is primarily chemical", and not mechanical.

Four experiments were run on samples of Calico Hills Tuff [15] at essentially the same test conditions (unconfined, 23°C, 10^{-5} s^{-1}). These results are also presented in Table 8. In this study, two test specimens were fully saturated and two were room-dry. Similar to the Grouse Canyon study, the average strength for the water-saturated samples was approximately 23% less than for the room-dry samples.

Effects of Pressure

Confining Pressure

Thirteen sets of tests on intact samples from drill holes USW G-1 and UE-25a#u 1 have been run to examine the effects of confining pressure on failure strength [9,10,15,18]. The experimental data were fit by linear regression of ultimate stress on to confining pressure and then transformed to the Coulomb equation in the same manner as described by Olsson and Jones [10]. The Coulomb failure criteria is as follows :

$$\tau = \tau_0 + \sigma_n(tan\ \phi),$$

where τ is shear stress, τ_0 is cohesion, σ_n is normal stress, and ϕ is the angle of internal friction. These results are summarized in Table 9 and plotted in Figures 15A-15M.

Five of the test sets were run with room-dry samples. These data illustrate a relatively small range of cohesion values (10.2-17.5 MPa) and a large range of friction angles (25.0-67.0°). Three sets of Calico Hills samples were deformed fully saturated, but with no exit for pore fluid during the course of the tests (i.e. "undrained"). The resulting ranges, and magnitudes, of Coulomb parameters are quite small, with cohesion and friction angle ranging from 9.7 to 13.2 MPa and 4.8 to 7.8°, respectively. The three remaining test series were performed saturated and drained, with two sets at room temperature and one set at 200°C. As a result, no trends can be observed due to the wide variations in test conditions.

Figures 16 and 17 are plots of cohesion and angle of internal friction, respectively, against effective porosity. Even with the wide variations in experimental conditions, the general inverse relationship between each of the Coulomb parameters and effective porosity is quite evident.

Pore Pressure

To date, only one series of tests has investigated the effects of pore fluid pressure on Yucca Mountain tuffs. Olsson [9] reported two test sets on Bullfrog samples deformed in compression at effective pressures of 5, 12.5 and 20.7 MPa; a temperature of 200°C; and a nominal strain rate of 10^{-4} s^{-1}. Four experiments were run on dry samples and three on saturated specimens with pore pressures of 5, 5 and 3.4 MPa. Considering the expected strength decrease in the saturated sample test data (i.e., water-weakening), the curve trends and ultimate strengths from tests run at the same effective pressure were very similar to each other. As a result, it is assumed that the concept of effective stress (i.e., $P_e = P_c - P_p$) holds for tuff, as it has been shown by Handin and others [2] to hold for many other porous rock types (e.g. sandstone, porous limestone, etc.).

Effects of Temperature

Three studies [9,10,20] refer to experimental data on tuff at elevated temperatures. The mechanical test results are summarized in Table 10.

In general, ultimate strength is inversely related to temperature, as would be expected. More specifically, the higher porosity (> 25%) ash fall tuffs decrease in strength 30 to 40% when the experimental temperature is increased from 23 to 200°C. One experimental series [20], however, found no difference in strength between two welded tuff samples (approximately 10% porosity) from Rainier Mesa deformed at 23 and 200°C.

Effects of Rate

Tests have been run at a range of laboratory strain rates (10^{-7} to 10^{-2} s^{-1}) to study the effects of changes in rate on mechanical properties. The data from three series of experiments on site-specific tuffs [14,15,16] are listed in Table 11 and presented in Figures 18A-18C, while the results from two series on tuffs from Rainier Mesa [10] are listed in Table 8 and presented in Figure 14.

The Tram (Figure 18A) and two Grouse Canyon (Figure 14) test series resulted in average strength decreases of approximately seven percent per decade decrease in strain rate. The decrease was somewhat less (about four percent per decade) for the Calico Hills (Figure 18B) tests. The Topopah Spring (Figure 18C) sequence of experiments resulted in no definitive rate effect on strength. It is believed that this result was due to physical property and mineralogical variability of the samples tested. The test specimens were taken from USW G-1 core over the depth range 371.3-390.0 m, and therefore probably had a wide range of physical and mineralogical characteristics, resulting in the large data scatter.

Estimate of Average and Limit Mechanical Properties

In order to aid in the numerical modeling of the Yucca Mountain tuff response to thermal and mechanical loading, the tuff sequence has been divided into nine thermal-mechanical zones [3] (see Figure 19). The zone boundaries were defined to reflect changes in mineralogical and bulk-rock properties (hence, significant changes in the mechanical properties) and are not always the same as the formal (geologic) stratigraphic divisions.

Lists of the input mechanical properties for each zone, and for the average and limit cases, are given in Tables 12 and 13. The elastic moduli and strength values were calculated using the parameters from previously discussed fits to the existing data, combined with the known average and limit bulk-rock properties [11,12]. The limit physical properties were defined as "worst-case" values, at two standard deviations below the mean. The angle of internal friction values were determined by using an estimated linear relationship with effective porosity, then these results, together with the unconfined compressive strength values, were used to back calculate the appropriate cohesion parameters. As a double check, the calculated cohesions were compared with the experimentally determined values and found to be reasonable.

Summary

Over two hundred and fifty mechanical experiments on tuff from Yucca Mountain have been performed. Other deformational tests have also been run on similar silicic tuff from Rainier Mesa. These data have been presented and analyzed for variations in elastic and strength properties with changes in porosity, effective porosity, grain density, zeolitization, water saturation, confining pressure, pore pressure, temperature, and strain rate.

A power-law model has been used to fit the elastic and strength data from unconfined compressive tests to bulk-rock properties. The results show that effective porosity is the best predictor of unconfined compressive strength and Young's modulus, especially when the data is divided on the basis of zeolitization. For Poisson's ratio, a combination of effective porosity and grain density fits the data best. In addition, the unconfined tensile strength data (from Brazilian tests) has been linearly fit to porosity as a first-order predictive tool.

Water saturated samples were found to be 23 and 30% weaker than room-dry and oven-dry samples, respectively. This water-weakening effect is an expected result for all silicate rocks, and in this case appears to be chemical, and not mechanical, in nature.

The pressure test series run to date were fit by the Coulomb failure criteria. These results, although obtained under a wide variety of experimental conditions, have shown that both the angle of internal friction and cohesion are inversely related to effective porosity. One sequence of experiments has indicated that the law of effective stress holds for the porous tuffs.

The strengths of the higher porosity tuffs are 30 to 40% lower at 200°C than at room temperature (about 23°C). The strengths of the lower porosity tuffs, however, may be affected very little by the same temperature variation.

Under normal laboratory axial strain rates (10^{-7} to 10^{-2} s^{-1}), an average decrease in ultimate strength of four to seven percent per decade decrease in strain rate has been observed.

References

1. **Blacic, J., Carter, J., Halleck, P., Johnson, P., Shankland, T., Anderson, R., Spicochi, K., and Heller, A.**
   Effects of Long-Term Exposure of Tuffs to High-Level Nuclear Waste-Repository Conditions LA-9174-PR, Los Alamos National Laboratory, Los Alamos, NM, Feb 1982
2. **Handin, J., Hager, R., Friedman, M., and Feather, J.**
   Experimental Deformation of Sedimentary Rocks under Confining Pressure : Pore Pressure Tests A.A.P.G. Bullet., V.47, n.5, 717-755, May 1963
3. **Langkopf, B. S.**
   Discussion of Thermomechanical Cross-Section CC ′ as Given to RE/SPEC for Far-Field Unit Selection Calculations Unclassified memorandum to Distribution, Sandia National Laboratories, Albuquerque, NM, Jul 23, 1982
4. **Lappin, A. R.**
   Bulk and Thermal Properties of the Functional Tuffaceous Beds, Here Defined to Include the Basal Topopah Spring, All of the Tuffaceous Beds of Calico Hills, and the Upper Portion of the Prow Pass Unclassified memorandum to Distribution, Sandia National Laboratories, Albuquerque, NM, Mar 26, 1982
5. **Lappin, A. R.**
   Bulk and Thermal Properties for the Welded, Devitrified Portions of the Bullfrog and Tram Members, Crater Flat Tuff Unclassified memorandum to Distribution, Sandia National Laboratories, Albuquerque, NM, Apr 19, 1982
6. **Lappin, A. R.**
   Bulk and Thermal Properties of the Potential Emplacement Horizon Within the Densely Welded, Devitrified Portion of the Topopah Spring Member of the Paintbrush Tuff Unclassified memorandum to Distribution, Sandia National Laboratories, Albuquerque, NM, May 25, 1982
7. **Lappin, A. R., VanBuskirk, R. G., Enniss, D. O., Butters, S. W., Prater, F. M., Muller, C. B., and Bergosh, J. L.**
   Thermal Conductivity, Bulk Properties, and Thermal Stratigraphy of Silicic Tuffs From the Upper Portion of Hole USW G-1, Yucca Mountain, Nye County, Nevada SAND81-1873, Sandia National Laboratories, Albuquerque, NM, Mar 1982
8. **Olsson, W. A.**
   Comparative Test Sequence Documentation Unclassified memorandum to A. R. Lappin, Sandia National Laboratories, Albuquerque, NM, Jul 1, 1981
9. **Olsson, W. A.**
   Effects of Elevated Temperature and Pore Pressure on the Mechanical Behavior of Bullfrog Tuff SAND81-1664, Sandia National Laboratories, Albuquerque, NM, Feb 1982

10. **Olsson, W. A. and Jones, A. K.**
Rock Mechanics Properties of Volcanic Tuffs from the Nevada Test Site SAND80-1453, Sandia National Laboratories, Albuquerque, NM, Nov 1980
11. **Peters, R. R. and Lappin, A. R.**
Revised Far-Field Thermomechanical Calculations for Four Average Property Cases Unclassified memorandum to T. Brandshaug, Sandia National Laboratories, Albuquerque, NM, Aug 17, 1982
12. **Peters, R. R. and Lappin, A. R.**
Revised Far-Field Thermomechanical Calculations for Four Limit Property Cases Unclassified memorandum to T. Brandshaug, Sandia National Laboratories, Albuquerque, NM, Sep 22, 1982
13. **Price, R. H., Jones, A. K., and Nimick, K. G.**
Uniaxial Compression Test Series on Bullfrog Tuff SAND82-0481, Sandia National Laboratories, Albuquerque, NM, Apr 1982
14. **Price, R. H. and Nimick, K. G.**
Uniaxial Compression Test Series on Tram Tuff SAND82-1055, Sandia National Laboratories, Albuquerque, NM, Jul 1982
15. **Price, R. H. and Jones, A. K.**
Uniaxial and Triaxial Compression Test Series on Calico Hills Tuff SAND82-1314, Sandia National Laboratories, Albuquerque, NM, November 1982
16. **Price, R. H., Nimick, K. G., and Zirzow, J. A.**
Uniaxial and Triaxial Compression Test Series on Topopah Spring Tuff SAND82-1723, Sandia National Laboratories, Albuquerque, NM, Nov 1982
17. **Sheldon, D. D.**
Soil Mechanical Properties as a Function of Physical Properties Unclassified memorandum to R. H. Price, Sandia National Laboratories, Albuquerque, NM, Jul 30, 1982
18. **Terra Tek, Inc.**
Tram, Bullfrog, and Calico Hills Tuff Mechanical Data Personal communication, 1982
19. **Waters, A. C. and Carroll, P. R. (eds.)**
Preliminary Stratigraphic and Petrologic Characterization of Core Samples from USW G-1, Yucca Mountain, Nevada La-8840-MS, Los Alamos National Laboratory, Los Alamos, NM, 1981
20. **Wawersik, W. R.**
Compression Tests on Ashfall Tuff and Welded Tuff at Ambient Temperature and 200°C Unclassified memorandum to L. D. Tyler, Sandia National Laboratories, Albuquerque, NM, Mar 27, 1978

Table 1. Symbols, Conventions and Units

SYMBOL	DEFINITION	UNITS
σ_1 , σ_2 , σ_3	Principal stresses; compressive stresses are positive	MPa
ϵ_1 , ϵ_2 , ϵ_3	Principal strains; compressive strains are positive	%
P_c	Confining pressure	MPa
P_p	Pore pressure	MPa
P_e	Effective pressure ($P_e = P_c - P_p$)	MPa
$\Delta\sigma$	Differential stress ($\sigma_1 - \sigma_3$ or $\sigma_1 - P_e$)	MPa
C_0	Unconfined (uniaxial) compressive strength	MPa
T_0	Unconfined (uniaxial) tensile strength	MPa
$(\Delta\sigma)_u$	Ultimate (maximum or peak) differential stress	MPa
$(\epsilon_1)_u$	Greatest principal strain at the ultimate differential stress	%
$\dot{\epsilon}$	Nominal strain rate	s^{-1}
T	Temperature	°C
S	Saturation of test sample (Y : fully saturated, R : room dry , N : oven dried)	—
D	Drained experiment (i.e., the sample was allowed to vent pore fluids during the experiment) (Y : yes , N : no)	—
E	Elastic constant : Young's modulus	GPa
ν	Elastic constant : Poisson's ratio	—
$\tau = \tau_0 + \sigma_n(\tan\phi)$	Coulomb failure criteria	
τ	Shear stress	MPa
τ_0	Cohesion (inherent shear strength)	MPa
σ_n	Normal stress	MPa
ϕ	Angle of internal friction	°
$\tan\phi$	Coefficient of internal friction	—
n	Effective porosity (porosity + clay volume)	%
ρ_g	Average grain density	Mg/m^3

Table 2. Abbreviations

ABBREVIATION	DEFINITION
SNLA	Sandia National Laboratories - Albuquerque
TT	Terra Tek, Inc.
NNWSI	Nevada Nuclear Waste Storage Investigations
NTS	Nevada Test Site
RM	Rainier Mesa, Nevada Test Site
Tbrg	Grouse Canyon Member of the Belted Range Tuff
YM	Yucca Mountain, Nevada Test Site
Tpc	Tiva Canyon Member of the Paintbrush Tuff
Tpt	Topopah Spring Member of the Paintbrush Tuff
Tc	Tuffaceous beds of Calico Hills
Tcfp	Prow Pass Member of the Crater Flat Tuff
Tcfb	Bullfrog Member of the Crater Flat Tuff
Tcft	Tram Member of the Crater Flat Tuff
G1	Drill hole USW G-1 at Yucca Mountain
A1	Drill hole UE-25a#1 at Yucca Mountain
Model 1	$\text{Log } Y = B_0 + B_1 \text{ Log } X$
Model 2	$\text{Log } Y = B_0 + B_1 \text{ Log } X_1 + B_2 \text{ Log } X_2$
X	Effective porosity or Grain density
X_1	Effective porosity
X_2	Grain density
Y	Young's modulus or Poisson's ratio
B_0 , B_1 , B_2	Fitting parameters
Data set A	All tuff samples
Data set B	Zeolitized tuff samples only ($\rho_g \leq 2.52\ Mg/m^3$)
Data set C	Non-zeolitized tuff samples only ($\rho_g > 2.52\ Mg/m^3$)
$\bar{d}$	Average difference between comparative values
F.S.	Fit significance (S : significant $\Rightarrow \alpha \leq .05$ NS : not significant $\Rightarrow \alpha > .05$)
S_ϵ	Standard Error
R^2	Index of determination

Table 3. Model Fits to Young's Modulus Data

LAB (SNLA , TT)	X (n , ρ_g)	Y (C_0 , E , ν)	DATA SET (A , B , C)	MODEL (1 , 2)	F. S. (S , NS)	B_0	B_1	B_2	S_ϵ of Y	R^2
SNLA	n	E	A	1	S	3.641	-1.800	-	.124	.676
SNLA	ρ_g	E	A	1	S	-.3940	3.411	-	.212	.056
SNLA	n , ρ_g	E	A	2	S	4.766	-1.949	-2.241	.122	.696
SNLA	n	E	B	1	S	4.375	-2.245	-	.127	.708
SNLA	ρ_g	E	B	1	NS	-	-	-	-	-
SNLA	n , ρ_g	E	B	2	NS	-	-	-	-	-
SNLA	n	E	C	1	S	4.108	-2.155	-	.101	.730
SNLA	ρ_g	E	C	1	NS	-	-	-	-	-
SNLA	n , ρ_g	E	C	2	S	.4652	-2.433	9.727	.085	.813
TT	n	E	A	1	S	2.648	-1.178	-	.217	.213
TT	ρ_g	E	A	1	NS	-	-	-	-	-
TT	n , ρ_g	E	A	2	NS	-	-	-	-	-
TT	n	E	B	1	S	2.970	-1.347	-	.178	.291
TT	ρ_g	E	B	1	NS	-	-	-	-	-
TT	n , ρ_g	E	B	2	NS	-	-	-	-	-
TT	n	E	C	1	S	3.799	-2.017	-	.229	.306
TT	ρ_g	E	C	1	NS	-	-	-	-	-
TT	n , ρ_g	E	C	2	NS	-	-	-	-	-

Table 4. Model Fits to Poisson's Ratio Data

LAB (SNLA , TT)	X (n , ρ_g)	Y (C_0 , E , ν)	DATA SET (A , B , C)	MODEL (1 , 2)	F. S. (S , NS)	B_0	B_1	B_2	S_ϵ of Y	R^2
SNLA	n	ν	A	1	NS	-	-	-	-	-
SNLA	ρ_g	ν	A	1	S	-2.364	4.138	-	.176	.135
SNLA	n , ρ_g	ν	A	2	S	-3.932	.6760	5.560	.169	.229
SNLA	n	ν	B	1	S	-2.385	1.067	-	.156	.291
SNLA	ρ_g	ν	B	1	NS	-	-	-	-	-
SNLA	n , ρ_g	ν	B	2	NS	-	-	-	-	-
SNLA	n	ν	C	1	NS	-	-	-	-	-
SNLA	ρ_g	ν	C	1	NS	-	-	-	-	-
SNLA	n , ρ_g	ν	C	2	NS	-	-	-	-	-
TT	n	ν	A	1	S	.1514	-.7310	-	.175	.139
TT	ρ_g	ν	A	1	S	-2.916	4.928	-	.172	.165
TT	n , ρ_g	ν	A	2	S	-1.698	-.4724	3.641	.168	.212
TT	n	ν	B	1	S	.1249	-.7330	-	.182	.104
TT	ρ_g	ν	B	1	NS	-	-	-	-	-
TT	n , ρ_g	ν	B	2	NS	-	-	-	-	-
TT	n	ν	C	1	NS	-	-	-	-	-
TT	ρ_g	ν	C	1	S	-5.919	12.16	-	.149	.192
TT	n , ρ_g	ν	C	2	S	-6.125	-.6321	14.84	.144	.265

Table 5. Comparative Statistics of SNLA-TT Elastic Moduli Data

	Calico Hills	**Bullfrog**	**Tram**	**All Data**
Variable (units)	$\bar{d}$ (F.S.)	$\bar{d}$ (F.S.)	$\bar{d}$ (F.S.)	$\bar{d}$ (F.S.)
E (GPa)	-1.81 (S)	3.66 (S)	1.60 (S)	1.19 (S)
ν	.13 (S)	.01 (NS)	.08 (S)	.07 (S)

Table 6. Model Fits to Unconfined Compressive Strength Data

LAB (SNLA , TT)	X (n , ρ_g)	Y (C_0 , E , ν)	DATA SET (A , B , C)	MODEL (1 , 2)	F. S. (S , NS)	B_0	B_1	B_2	S_ϵ of Y	R^2
SNLA	n	C_0	A	1	S	4.103	-1.724	-	.155	.553
SNLA	ρ_g	C_0	A	1	NS	-	-	-	-	-
SNLA	n , ρ_g	C_0	A	2	S	6.096	-2.008	-3.963	.147	.606
SNLA	n	C_0	B	1	S	5.728	-2.741	-	.132	.770
SNLA	ρ_g	C_0	B	1	NS	-	-	-	-	-
SNLA	n , ρ_g	C_0	B	2	NS	-	-	-	-	-
SNLA	n	C_0	C	1	S	4.579	-2.123	-	.114	.667
SNLA	ρ_g	C_0	C	1	NS	-	-	-	-	-
SNLA	n , ρ_g	C_0	C	2	S	.4797	-2.435	10.94	.097	.766
TT	n	C_0	A	1	S	3.827	-1.510	-	.167	.428
TT	ρ_g	C_0	A	1	S	.1652	3.542	-	.214	.061
TT	n , ρ_g	C_0	A	2	NS	-	-	-	-	-
TT	n	C_0	B	1	S	4.350	-1.821	-	.139	.550
TT	ρ_g	C_0	B	1	NS	-	-	-	-	-
TT	n , ρ_g	C_0	B	2	S	1.791	-1.862	6.756	.128	.635
TT	n	C_0	C	1	S	4.419	-1.951	-	.178	.406
TT	ρ_g	C_0	C	1	NS	-	-	-	-	-
TT	n , ρ_g	C_0	C	2	S	-.7916	-2.318	13.82	.162	.519

Table 7. Comparative Statistics of SNLA-TT Unconfined Compressive Strength Data

	Calico Hills	**Bullfrog**	**Tram**	**All Data**
Variable (units)	$\bar{d}$ (F.S.)	$\bar{d}$ (F.S.)	$\bar{d}$ (F.S.)	$\bar{d}$ (F.S.)
$(\Delta\sigma)_u$ (MPa)	-10.09 (S)	3.17 (S)	-18.62 (S)	-7.94 (S)
$(\epsilon_1)_u$ (%)	.001 (NS)	-.11 (S)	-.10 (S)	-.07 (S)

Table 8. Test Results on the Effects of Changes in Water Content

Location	Unit	Depth (m)	P_e (MPa)	T (°C)	$\dot{\epsilon}$ (s^{-1})	S (Y,R,N)	D (Y,N)	$(\Delta\sigma)_u$ (MPa)	$(\epsilon_1)_u$ (%)	E (GPa)	ν	Ref
YM	Tc	507.6 (G1)	0	23	10^{-5}	R	Y	41.0	.58	8.12	.29	15
YM	Tc	507.6 (G1)	0	23	10^{-5}	R	Y	32.7	.54	6.50	.31	15
YM	Tc	507.6 (G1)	0	23	10^{-5}	Y	Y	26.2	.50	6.86	.18	15
YM	Tc	507.6 (G1)	0	23	10^{-5}	Y	Y	34.1	.42	9.52	-	15
RM	Tbrg	-	0	23	10^{-2}	N	Y	175	-	25.9	-	10
RM	Tbrg	-	0	23	10^{-2}	N	Y	189	-	28.7	-	10
RM	Tbrg	-	0	23	10^{-2}	N	Y	177	-	28.4	-	10
RM	Tbrg	-	0	23	10^{-4}	N	Y	160	-	26.2	-	10
RM	Tbrg	-	0	23	10^{-4}	N	Y	155	-	28.5	-	10
RM	Tbrg	-	0	23	10^{-4}	N	Y	160	-	27.4	-	10
RM	Tbrg	-	0	23	10^{-6}	N	Y	135	-	27.4	-	10
RM	Tbrg	-	0	23	10^{-6}	N	Y	141	-	28.3	-	10
RM	Tbrg	-	0	23	10^{-6}	N	Y	134	-	29.5	-	10
RM	Tbrg	-	0	23	10^{-2}	Y	Y	142	-	26.1	-	10
RM	Tbrg	-	0	23	10^{-2}	Y	Y	114	-	22.8	-	10
RM	Tbrg	-	0	23	10^{-2}	Y	Y	118	-	23.8	-	10
RM	Tbrg	-	0	23	10^{-4}	Y	Y	112	-	24.8	-	10
RM	Tbrg	-	0	23	10^{-4}	Y	Y	122	-	25.3	-	10
RM	Tbrg	-	0	23	10^{-4}	Y	Y	102	-	24.0	-	10
RM	Tbrg	-	0	23	10^{-6}	Y	Y	81.1	-	25.9	-	10
RM	Tbrg	-	0	23	10^{-6}	Y	Y	110	-	25.4	-	10
RM	Tbrg	-	0	23	10^{-6}	Y	Y	91.8	-	26.8	-	10

Table 9. Parameter Values for the Coulomb Failure Criteria

Unit	Depth (G1) (m)	Depth (A1) (m)	P_e (MPa)	T (°C)	$\dot{\epsilon}$ (s^{-1})	S (Y,R,N)	D (Y,N)	τ_0 (MPa)	ϕ (°)	Ref
Tpc	-	26.7	0,10,20	23	10^{-4}	R	N	28.1	68	10
Tpt	-	220-381	0,10,20	23	10^{-4}	R	N	17.5	67	10
Tpt	352-362	-	0,5,10	23	10^{-5}	Y	Y	34.5	23.5	16
Tc	453.4	-	0,10,20	23	10^{-5}	Y	Y	10.2	11.1	15
Tc	453.4	-	0,10,20	23	10^{-5}	Y	N	10.6	7.81	15
Tc	-	454-516	0,20	23	10^{-4}	R	N	12.9	25	10
Tc	507.6	-	0,10	23	10^{-5}	R	N	10.2	32.2	15
Tc	507.6	-	0,10,20	23	10^{-5}	Y	N	13.2	6.81	15
Tc	508.4	-	0,10	23	10^{-5}	Y	N	9.67	4.78	15
Tcfp	-	600-614	0,20	23	10^{-4}	R	N	32.2	37	10
Tcfb	-	738-759	0,20	23	10^{-4}	R	N	12.1	43	10
Tcfb	759	-	5,12.5,20.7	200	10^{-4}	Y	Y	23.6	19.6	9
Tcfb	759	-	5,10,20.7	200	10^{-4}	N	Y	16.5	37.4	9

Table 10. Test Results on the Effects of Changes in Temperature

Location	Unit	Depth (m)	P_e (MPa)	T (°C)	$\dot{\epsilon}$ (s^{-1})	S (Y,R,N)	D (Y,N)	$(\Delta\sigma)_u$ (MPa)	$(\epsilon_1)_u$ (%)	E (GPa)	ν	Ref
YM	Tpt	225.2 (A1)	20.7	200	10^{-4}	R	Y	133	-	23.9	.15	10
YM	Tcfb	759 (G1)	5.0	200	10^{-4}	R	Y	87	-	16.5	-	9
YM	Tcfb	759 (G1)	5.0	200	10^{-4}	Y	Y	70	-	13.1	-	9
YM	Tcfb	759 (G1)	10.0	200	10^{-4}	R	Y	93	-	15.7	-	9
YM	Tcfb	759 (G1)	12.5	200	10^{-4}	Y	Y	83	-	17.8	-	9
YM	Tcfb	759 (G1)	20.7	200	10^{-4}	R	Y	119	-	17.6	-	9
YM	Tcfb	759 (G1)	20.7	200	10^{-4}	R	Y	149	-	20.5	-	9
YM	Tcfb	759 (G1)	20.7	200	10^{-4}	Y	Y	86	-	13.8	-	9
RM	-	-	0	23	10^{-5}	R	Y	36.3	.48	8.83	-	20
RM	-	-	0	200	10^{-5}	R	Y	22.6	.38	6.76	-	20
RM	-	-	10.3	23	10^{-5}	R	Y	53.5	1.05	8.83	.18	20
RM	-	-	10.3	23	10^{-5}	R	Y	51.9	1.06	8.76	.20	20
RM	-	-	10.3	200	10^{-5}	R	Y	35.6	.98	6.76	-	20
RM	Tbrg	-	0	23	10^{-5}	R	Y	120.7	-	-	-	20
RM	Tbrg	-	0	200	10^{-5}	R	Y	115.4	-	-	-	20

Table 11. Test Results on the Effects of Changes in Strain Rate

Location	Unit	Depth (G1) (m)	P_e (MPa)	T (°C)	$\dot{\epsilon}$ (s^{-1})	S (Y,R,N)	D (Y,N)	$(\Delta\sigma)_u$ (MPa)	$(\epsilon_1)_u$ (%)	E (GPa)	ν	Ref
YM	Tpt	372.5	0	23	10^{-2}	Y	Y	157.2	.48	29.2	.31	16
YM	Tpt	384.8	0	23	10^{-2}	Y	Y	149.7	.49	36.6	-	16
YM	Tpt	372.5	0	23	10^{-4}	Y	Y	133.8	.57	27.7	-	16
YM	Tpt	373.0	0	23	10^{-4}	Y	Y	157.2	.46	37.5	.25	16
YM	Tpt	371.3	0	23	10^{-6}	Y	Y	176.6	.51	40.8	.25	16
YM	Tpt	373.0	0	23	10^{-6}	Y	Y	156.6	.47	35.3	.21	16
YM	Tpt	390.0	0	23	10^{-6}	Y	Y	44.9	.41	22.9	.27	16
YM	Tc	508.4	0	23	10^{-3}	Y	Y	24.7	.61	5.41	.33	15
YM	Tc	508.4	0	23	10^{-3}	Y	Y	23.4	.58	5.45	-	15
YM	Tc	508.4	0	23	10^{-5}	Y	Y	25.4	.57	6.15	.36	15
YM	Tc	508.4	0	23	10^{-5}	Y	Y	16.7	.43	4.92	.18	15
YM	Tc	508.4	0	23	10^{-7}	Y	Y	21.5	.55	7.86	.21	15
YM	Tc	508.4	0	23	10^{-7}	Y	Y	19.9	.51	7.03	.22	15
YM	Tcft	976.2	0	23	10^{-2}	Y	Y	31.1	.52	6.63	-	14
YM	Tcft	976.2	0	23	10^{-2}	Y	Y	24.4	.50	5.17	-	14
YM	Tcft	976.2	0	23	10^{-4}	Y	Y	25.3	.50	6.42	-	14
YM	Tcft	976.2	0	23	10^{-4}	Y	Y	22.1	.32	8.76	-	14
YM	Tcft	976.2	0	23	10^{-4}	Y	Y	32.6	.44	8.97	.09	14
YM	Tcft	976.2	0	23	10^{-6}	Y	Y	14.5	.31	7.04	.30	14
YM	Tcft	976.2	0	23	10^{-6}	Y	Y	26.5	.50	8.26	.14	14

Table 12. Average-Case Mechanical Properties for each the of the Yucca Mountain Thermal/Mechanical Zones

Zone (#)	n* (%)	ρ_g* (Mg/m^3)	E (GPa)	ν	C_o (MPa)	T_o (MPa)	ϕ (°)	τ_o (MPa)
I	25	2.40	13.3	.13	49.3	6.0	20.8	16.1
IIA	27(12/15)	2.55	11.6	.20	43.2	4.3	19.5	14.4
IIB	17(12/5)	2.55	26.7	.14	95.9	12.8	26.0	28.5
III	25	2.39	13.3	.13	49.3	6.0	20.8	16.1
IVA	33	2.39	8.1	.16	30.6	0.1	15.6	10.9
IVB	25	2.50	13.3	.17	49.3	6.0	20.8	16.1
IVC	30	2.39	9.6	.15	36.0	1.8	17.5	12.4
VA	22	2.58	16.8	.18	61.5	8.6	22.7	19.3
VB	24	2.44	14.3	.14	52.9	6.9	21.4	17.0
VI	23	2.59	15.5	.19	56.9	7.7	22.1	18.1
VIIA	24	2.46	14.3	.15	52.9	6.9	21.4	17.0
VIIB	24	2.54	14.3	.18	52.9	6.9	21.4	17.0
VIIC	24	2.50	14.3	.16	52.9	6.9	21.4	17.0
VIII	19	2.64	21.8	.19	79.2	11.1	24.7	24.0
IX	17	2.62	26.7	.17	95.9	12.8	26.0	28.5

* From reference 11.

Table 13. Limit-Case Mechanical Properties for each of the Yucca Mountain Thermal/Mechanical Zones

Zone (#)	n* (%)	ρ_g* (Mg/m^3)	E (GPa)	ν	C_o (MPa)	T_o (MPa)	ϕ (°)	τ_o (MPa)
I	31	2.34	9.0	.13	34.0	0.9	16.9	11.9
IIA	41(16/25)	2.54	5.5	.26	21.0	0.1	10.4	8.2
IIB	21(16/5)	2.54	18.2	.16	66.6	9.4	23.4	20.7
III	31	2.33	9.0	.13	34.0	0.9	16.9	11.9
IVA	38	2.31	6.3	.14	24.0	0.1	12.3	9.0
IVB	39	2.34	6.0	.16	22.9	0.1	11.7	8.7
IVC	38	2.32	6.3	.15	24.0	0.1	12.3	9.0
VA	28	2.52	10.9	.19	40.6	3.5	18.8	13.7
VB	34	2.32	7.7	.14	29.0	0.1	14.9	10.5
VI	24	2.54	14.3	.18	52.9	6.9	21.4	17.0
VIIA	34	2.34	7.7	.14	29.0	0.1	14.9	10.5
VIIB	34	2.42	7.7	.17	29.0	0.1	14.9	10.5
VIIC	34	2.38	7.7	.16	29.0	0.1	14.9	10.5
VIII	25	2.54	13.3	.18	49.3	6.0	20.8	16.3
IX	23	2.56	15.5	.18	56.9	7.7	22.1	18.1

* From reference 12.

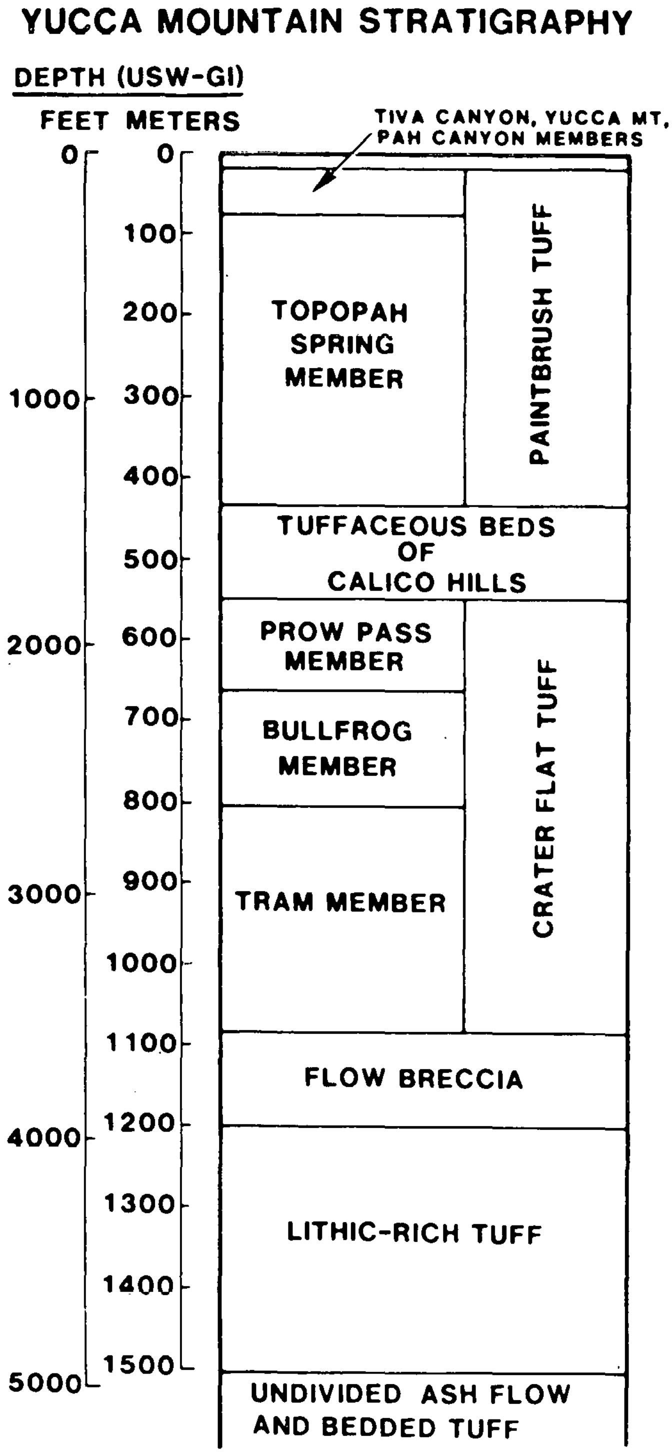

Figure 1
Yucca Mountain stratigraphic column at drillhole USW-G1.

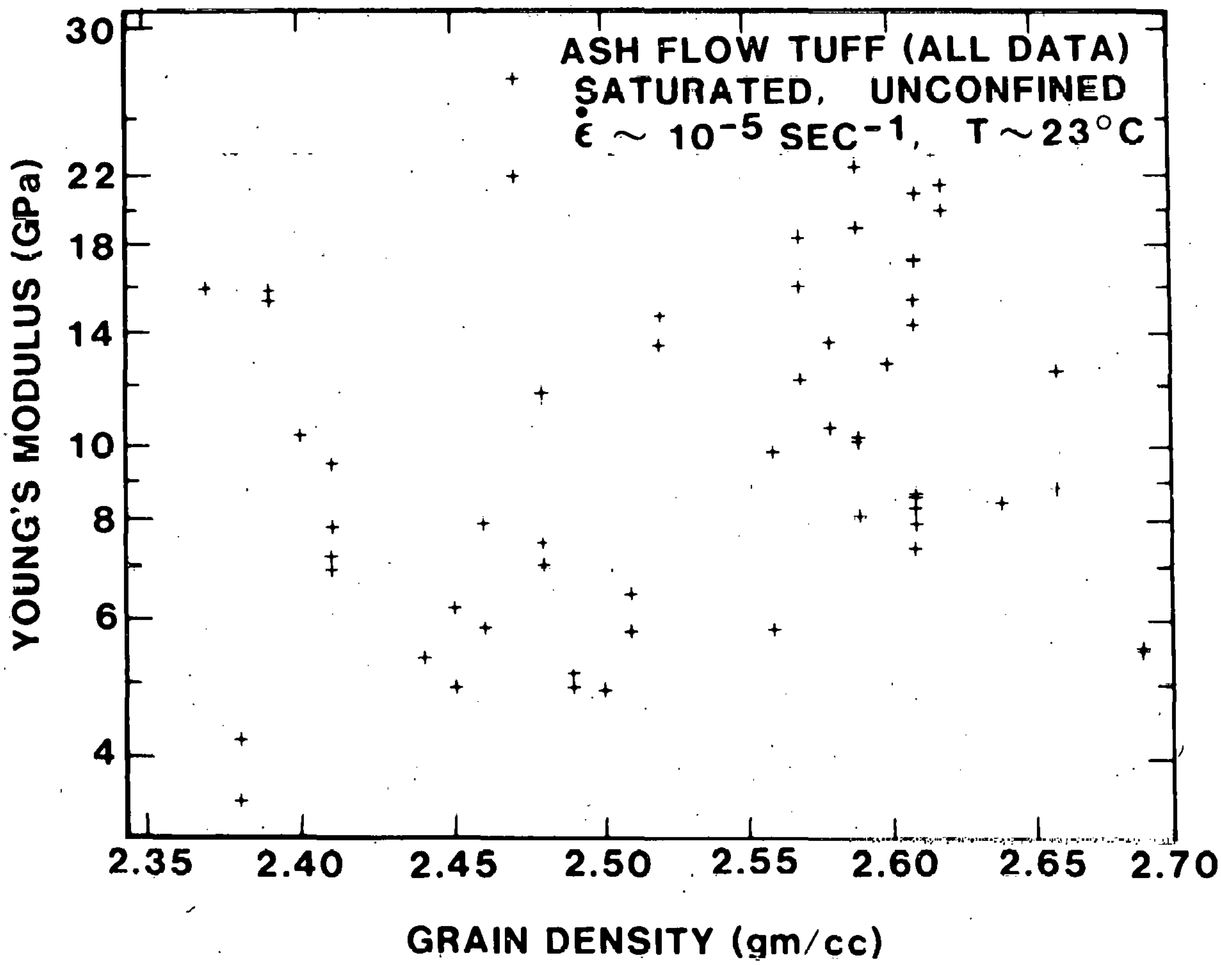

Figure 2

A plot of Young's modulus as a function of grain density for SNLA data from the Calico Hills, Bullfrog and Tram ash flow tuffs. All tests were run on saturated samples under unconfined, room temperature and 10^{-5} s^{-1} conditions.

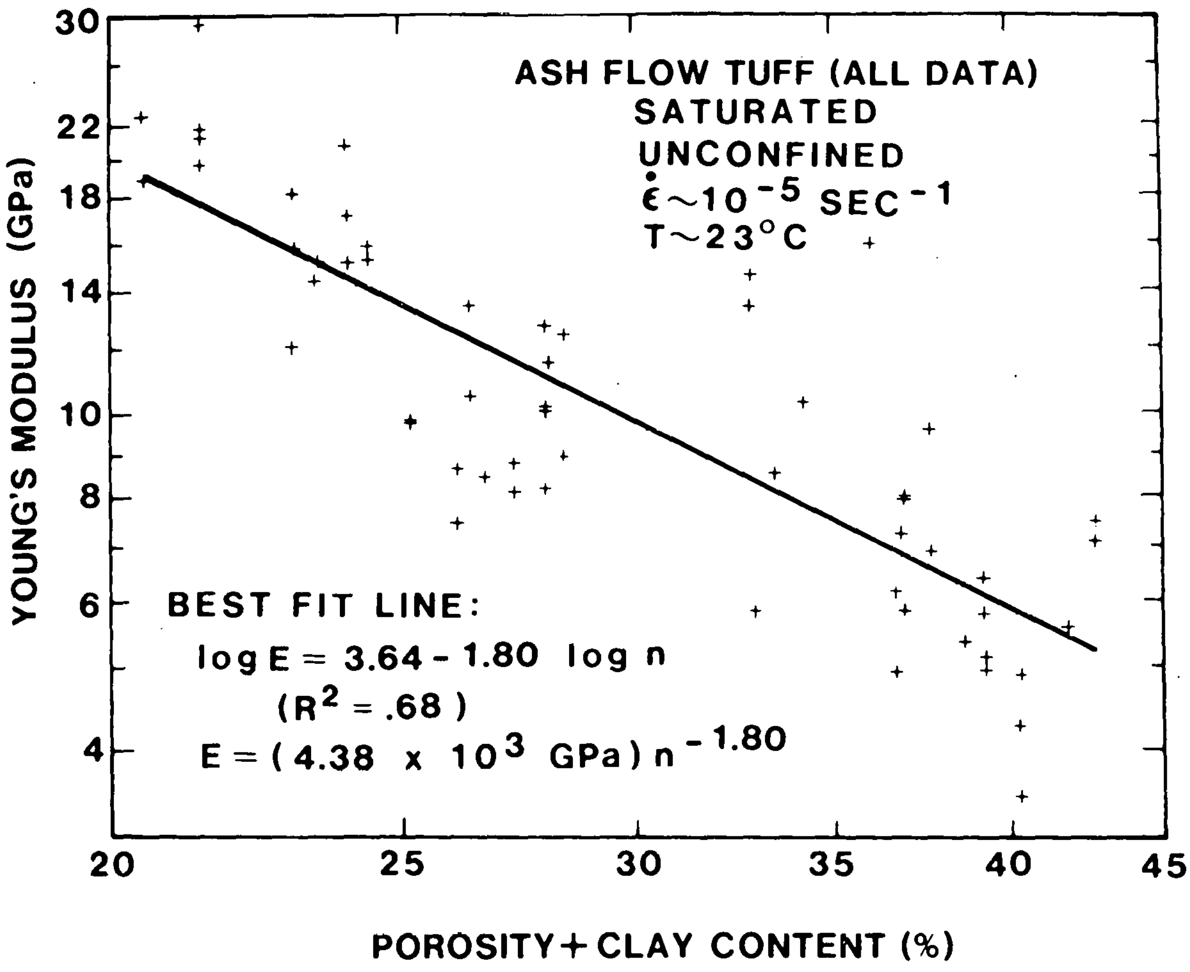

Figure 3

A plot of Young's modulus as a function of effective porosity for SNLA data from the Calico Hills, Bullfrog and Tram ash flow tuffs. All tests were run on saturated samples under unconfined, room temperature and 10^{-5} s^{-1} conditions.

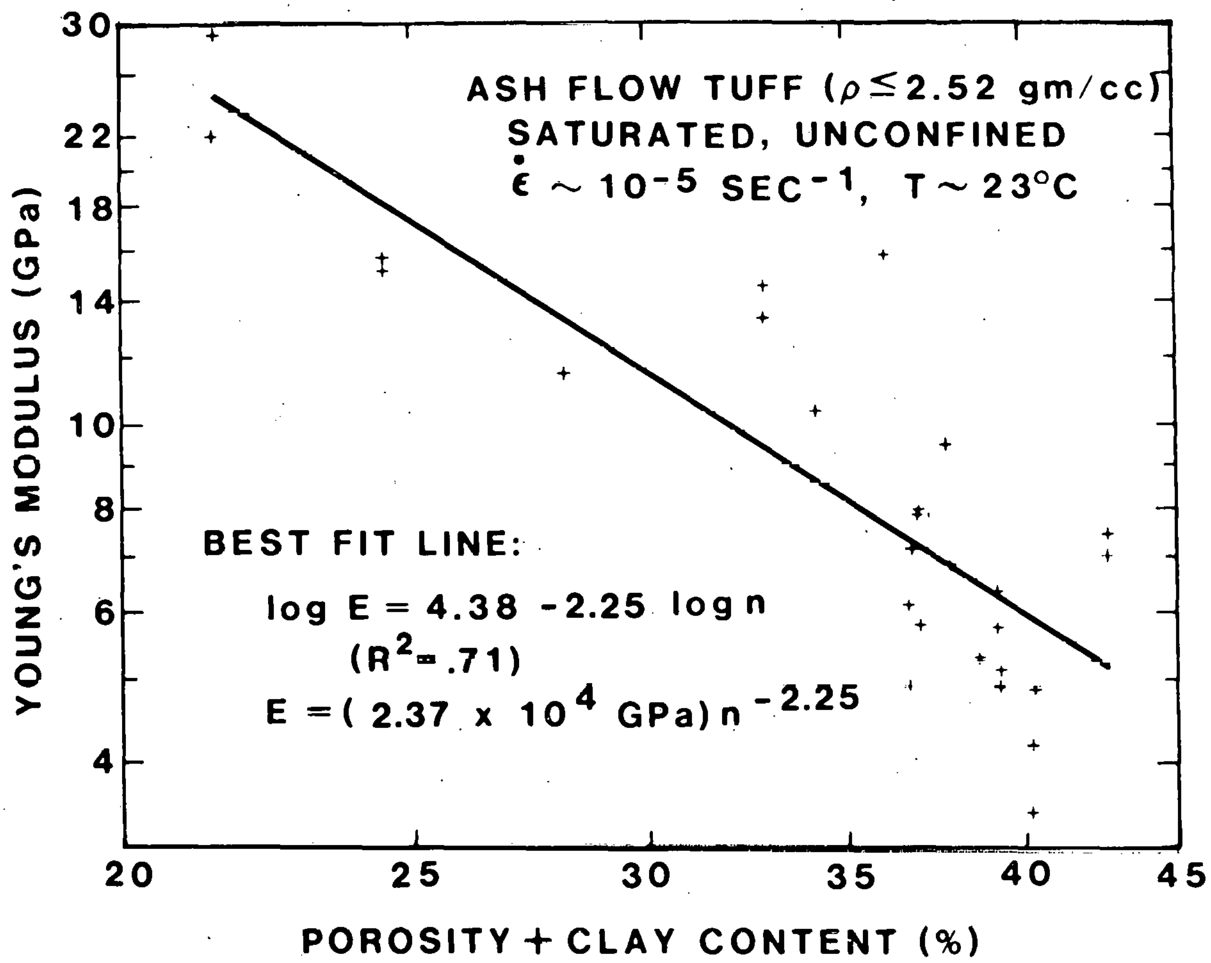

Figure 4A

Plot of Young's modulus as a function of effective porosity for zeolitized SNLA data from the Calico Hills, Bullfrog and Tram ash flow tuffs. All tests were run on saturated samples under unconfined, room temperature and 10^{-5} s^{-1} conditions.

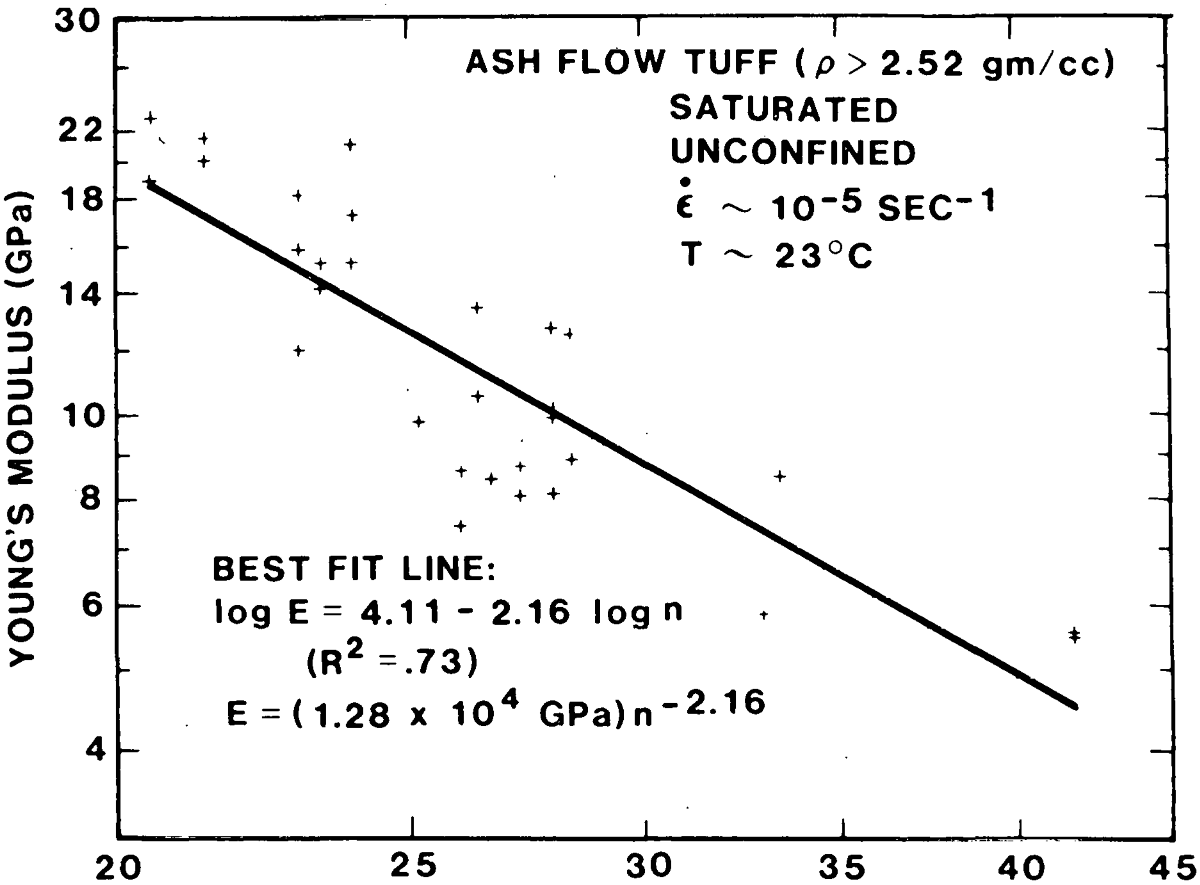

Figure 4B

Plot of Young's modulus as a function of effective porosity for non-zeolitized SNLA data from the Calico Hills, Bullfrog and Tram ash flow tuffs. All tests were run on saturated samples under unconfined, room temperature and 10^{-5} s^{-1} conditions.

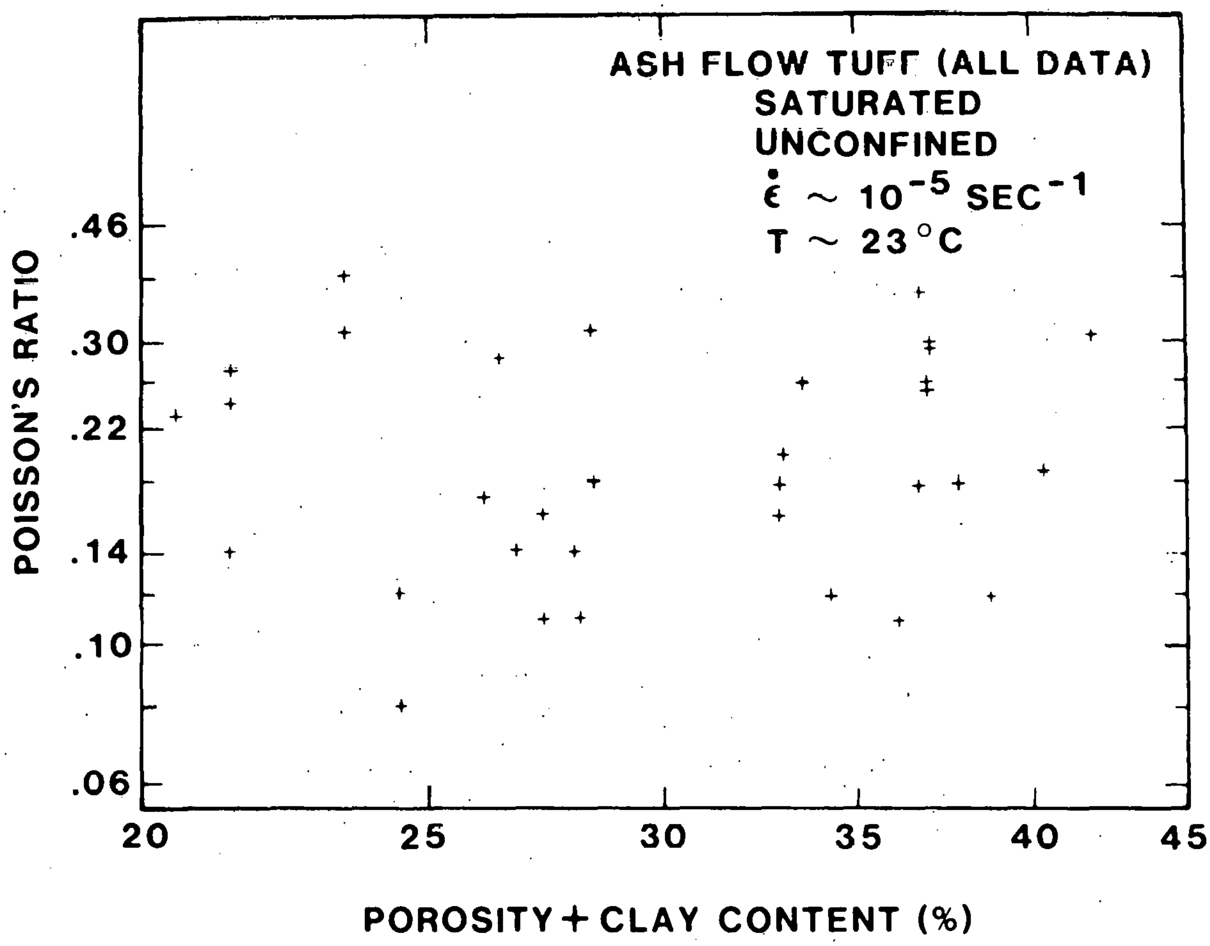

Figure 5

A plot of Poisson's ratio as a function of effective porosity for SNLA data from the Calico Hills, Bullfrog and Tram ash flow tuffs. All tests were run on saturated samples under unconfined, room temperature and 10^{-5} s^{-1} conditions.

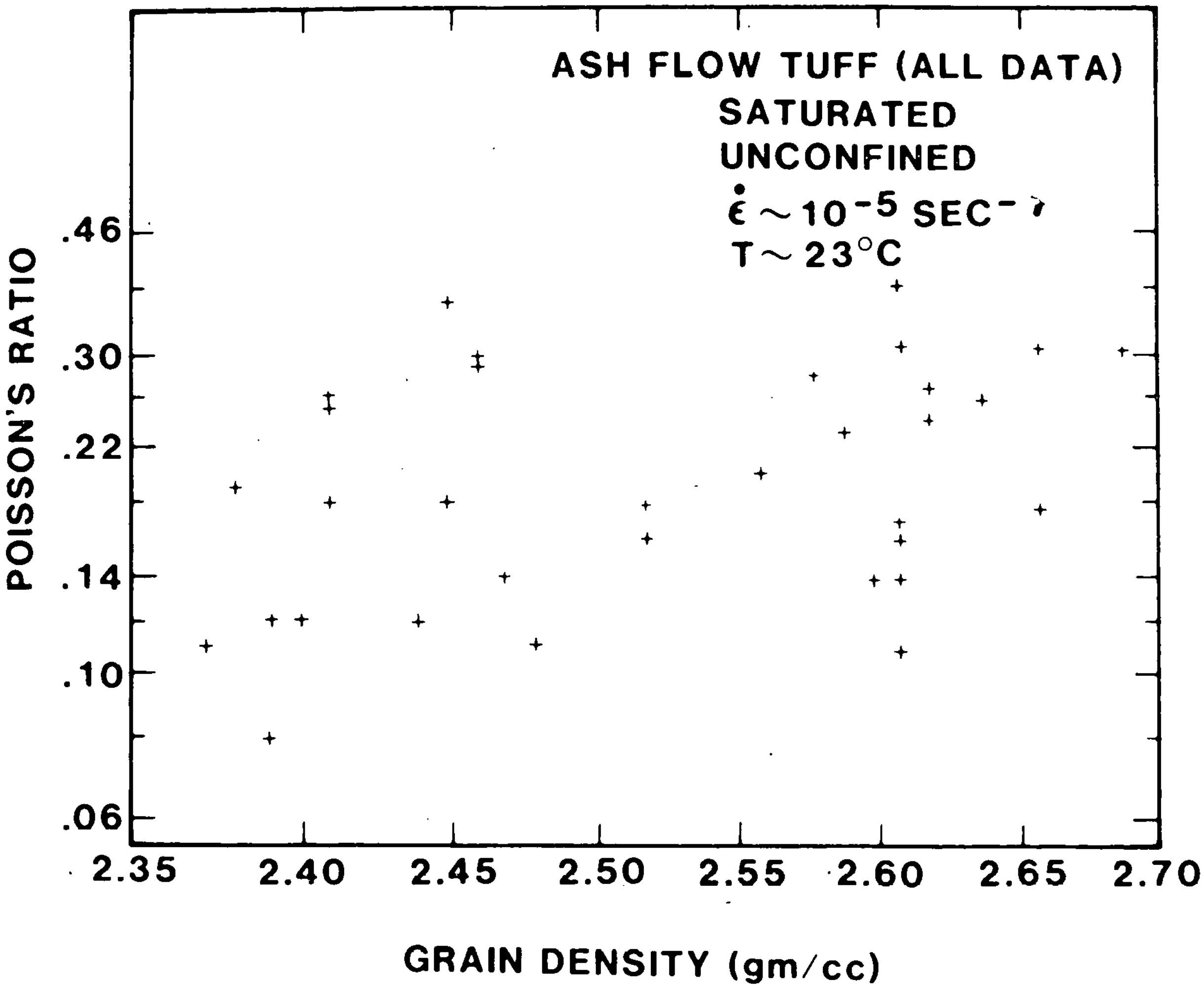

Figure 6

A plot of Poisson's ratio as a function of grain density for SNLA data from the Calico Hills, Bullfrog and Tram ash flow tuffs. All tests were run on saturated samples under unconfined, room temperature and 10^{-5} s^{-1} conditions.

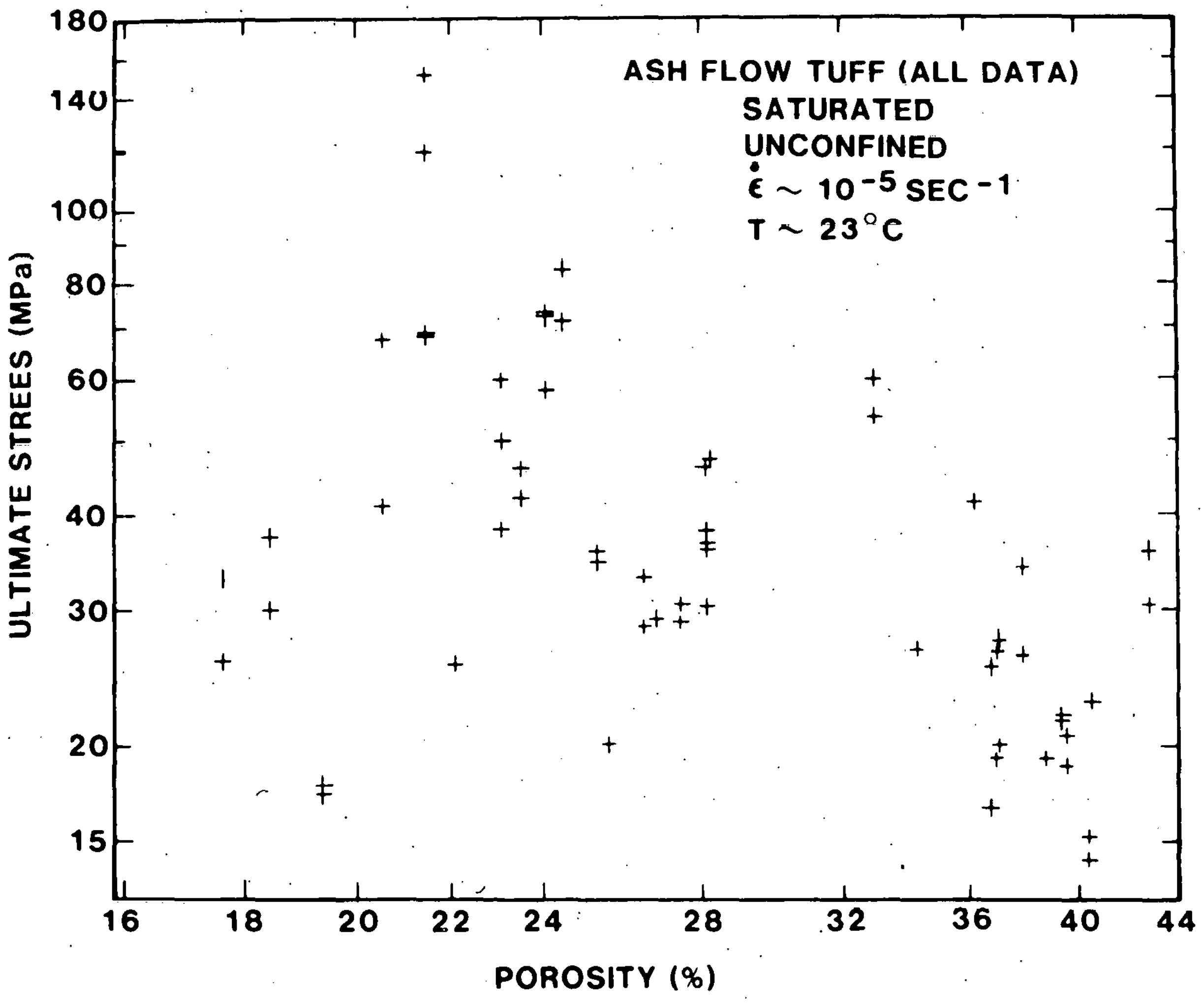

Figure 7

A plot of unconfined compressive strength as a function of porosity for SNLA data from the Calico Hills, Bullfrog and Tram ash flow tuffs. All tests were run on saturated samples under unconfined, room temperature and 10^{-5} s^{-1} conditions.

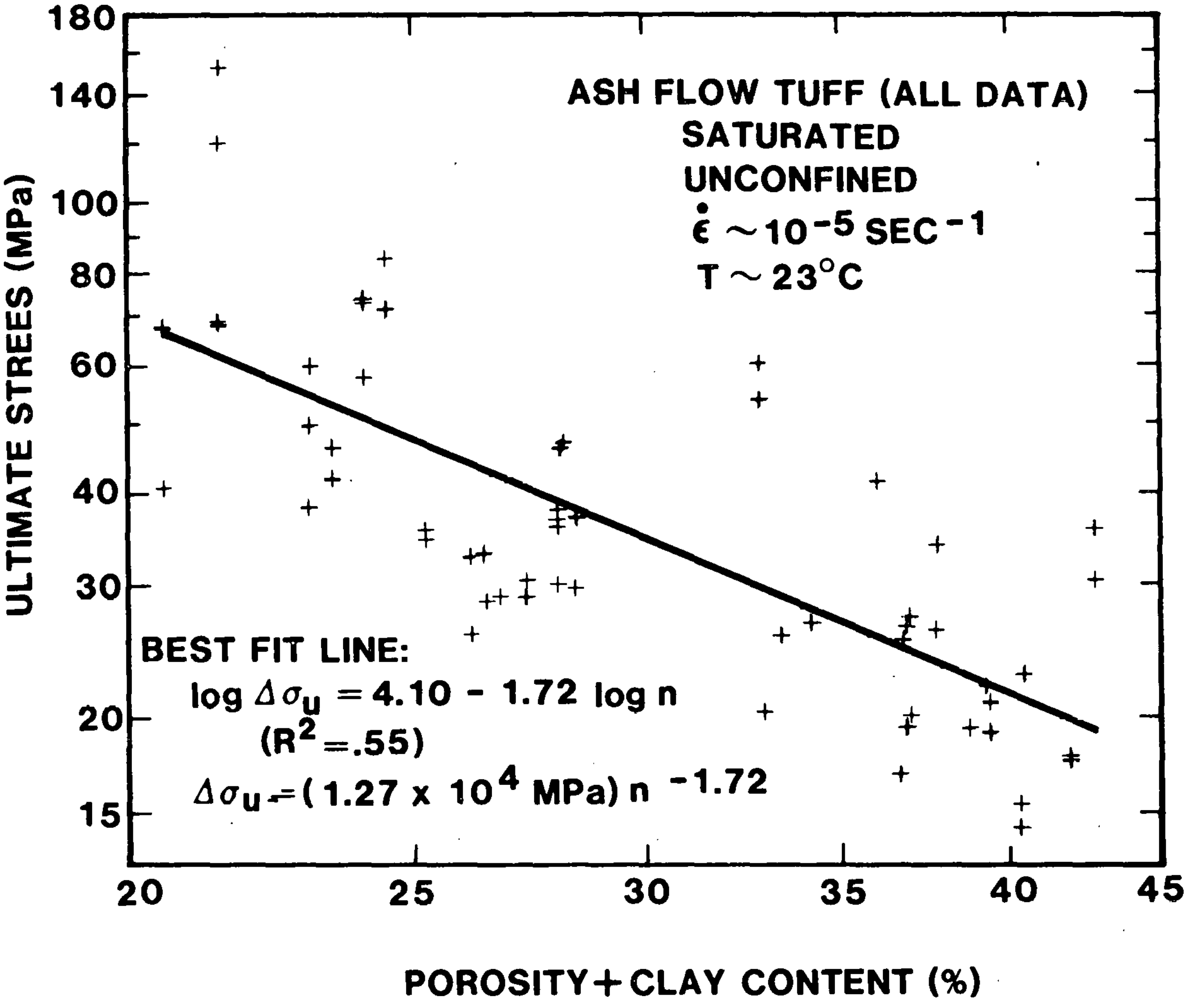

Figure 8

A plot of unconfined compressive strength as a function of effective porosity for SNLA data from the Calico Hills, Bullfrog and Tram ash flow tuffs. All tests were run on saturated samples under unconfined, room temperature and $10^{-5}\ s^{-1}$ conditions.

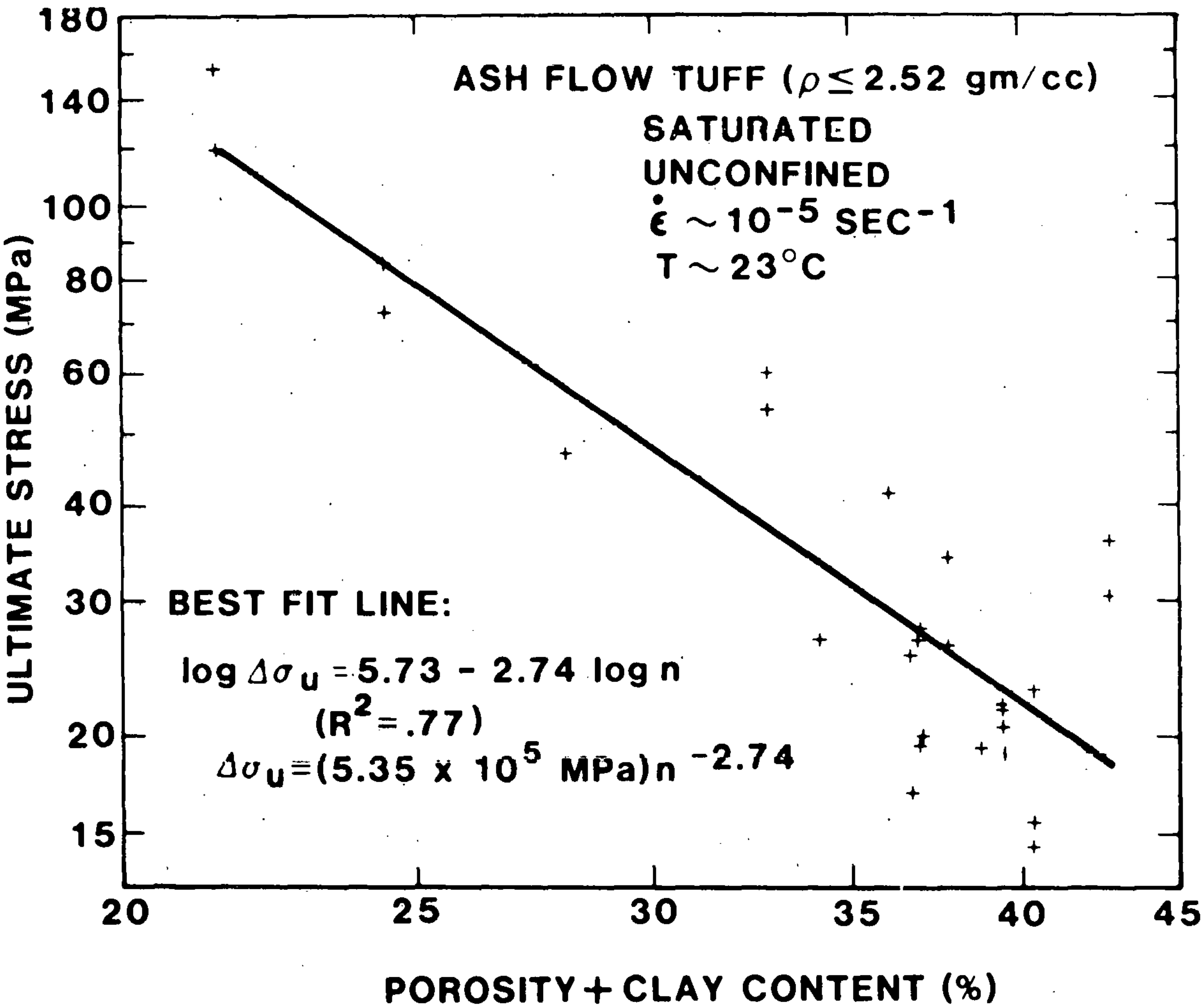

Figure 9A

Plots of unconfined compressive strength as a function of effective porosity for zeolitized SNLA data from the Calico Hills, Bullfrog and Tram ash flow tuffs. All tests were run on saturated samples under unconfined, room temperature and $10^{-5}\ s^{-1}$ conditions.

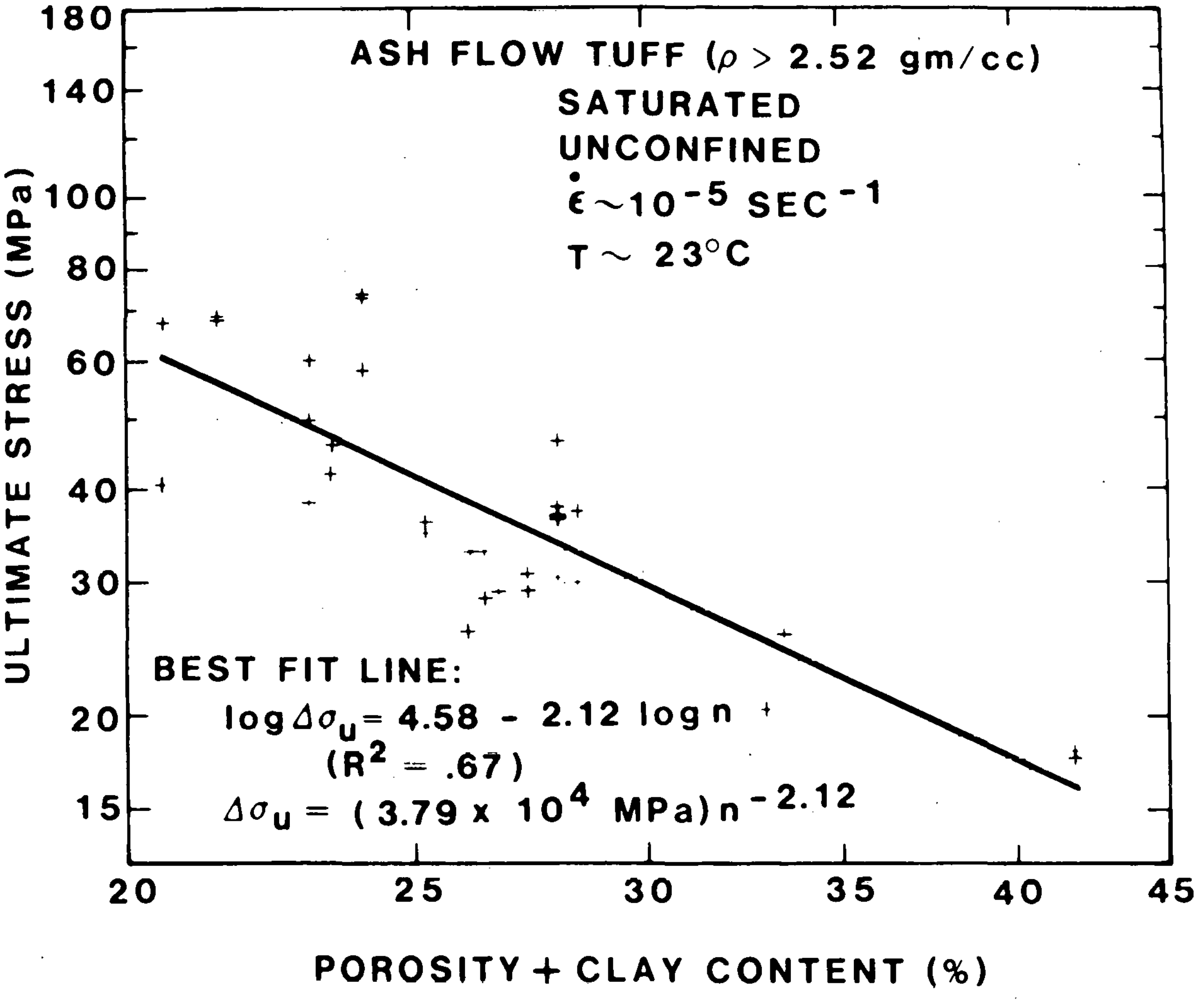

Figure 9B

Plots of unconfined compressive strength as a function of effective porosity for nonzeolitized SNLA data from the Calico Hills, Bullfrog and Tram ash flow tuffs. All tests were run on saturated samples under unconfined, room temperature and 10^{-5} s^{-1} conditions.

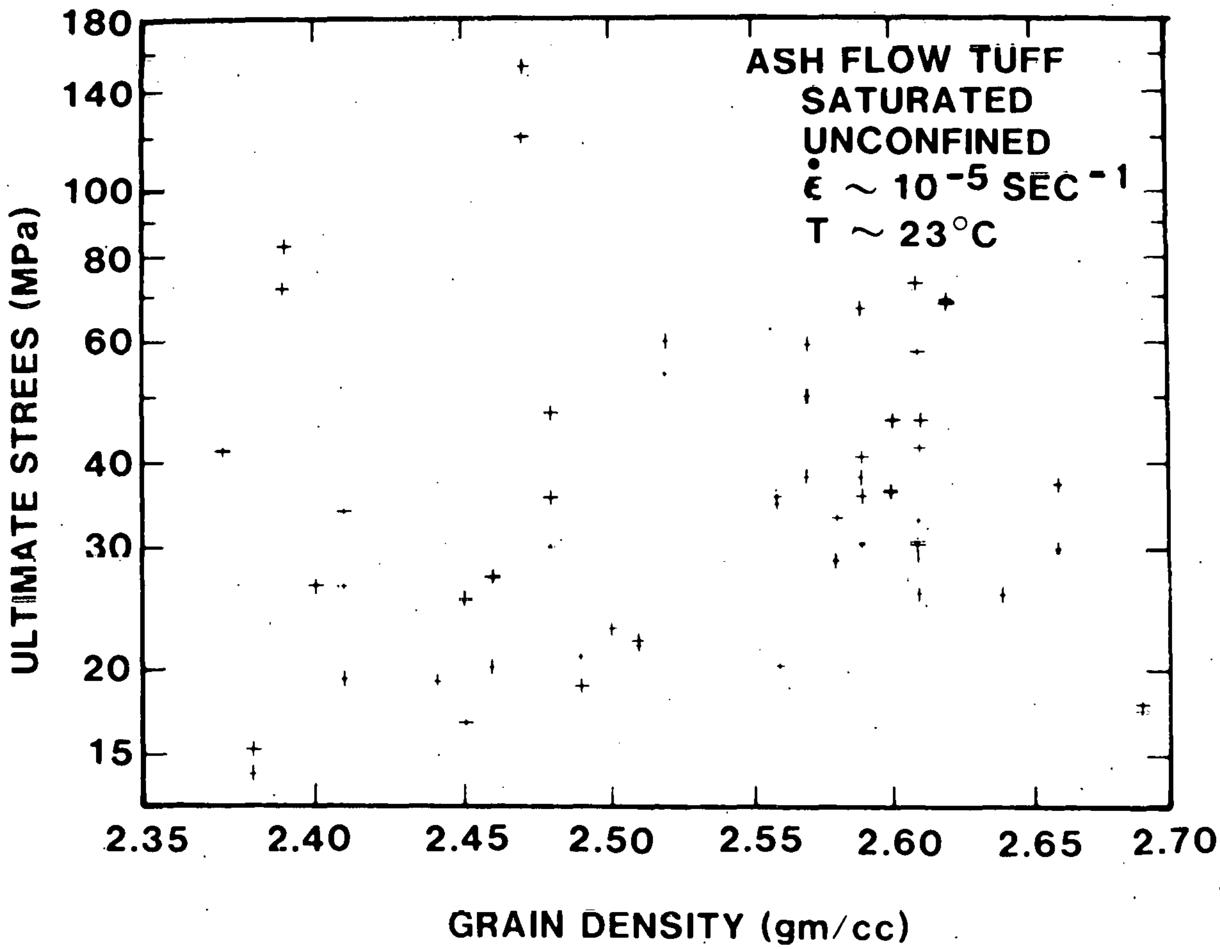

Figure 10

A plot of unconfined compressive strength as a function of grain density for SNLA data from the Calico Hills, Bullfrog and Tram ash flow tuffs. All tests were run on saturated samples under unconfined, room temperature and 10^{-5} s^{-1} conditions.

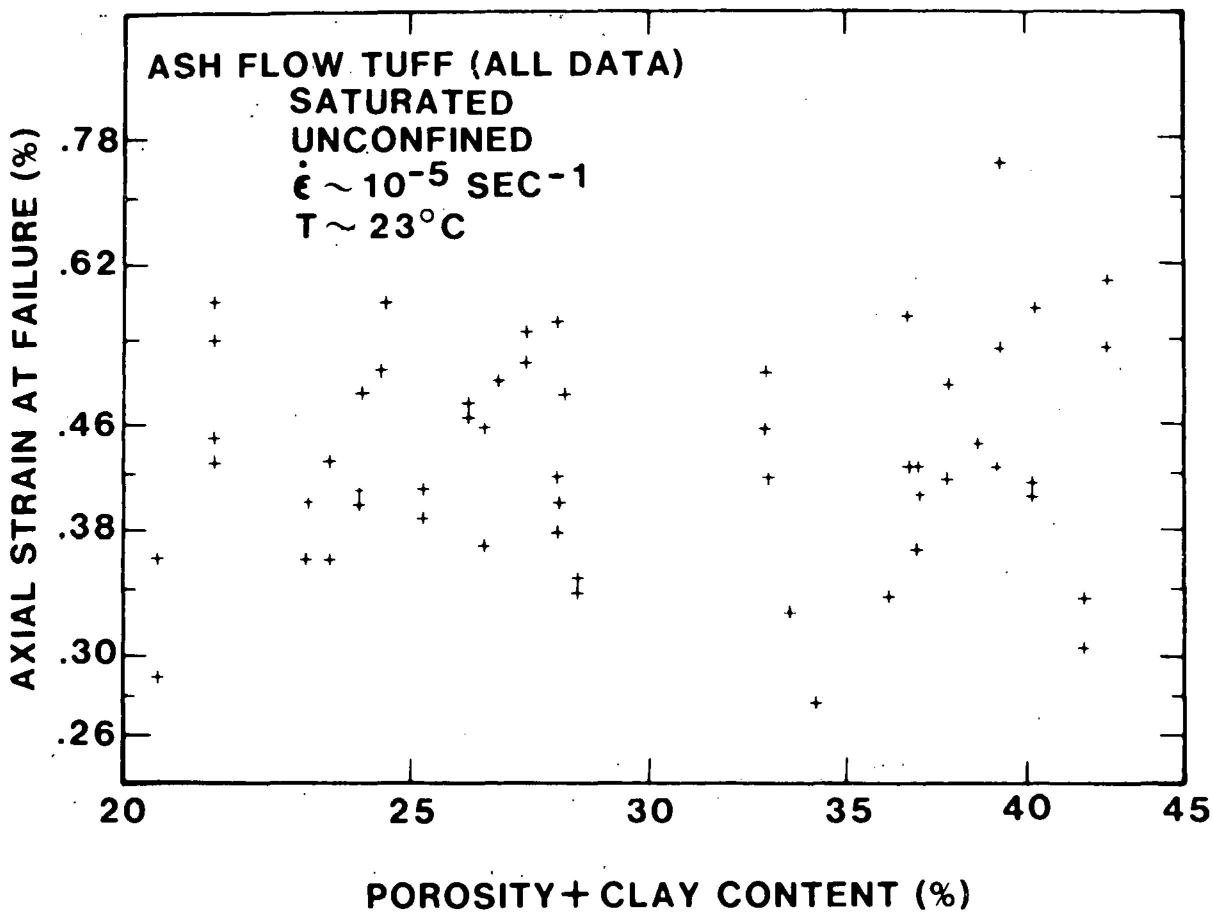

Figure 11

A plot of axial strain at failure as a function of effective porosity for SNLA data from the Calico Hills, Bullfrog and Tram ash flow tuffs. All tests were run on saturated samples under unconfined, room temperature and 10^{-5} s^{-1} conditions.

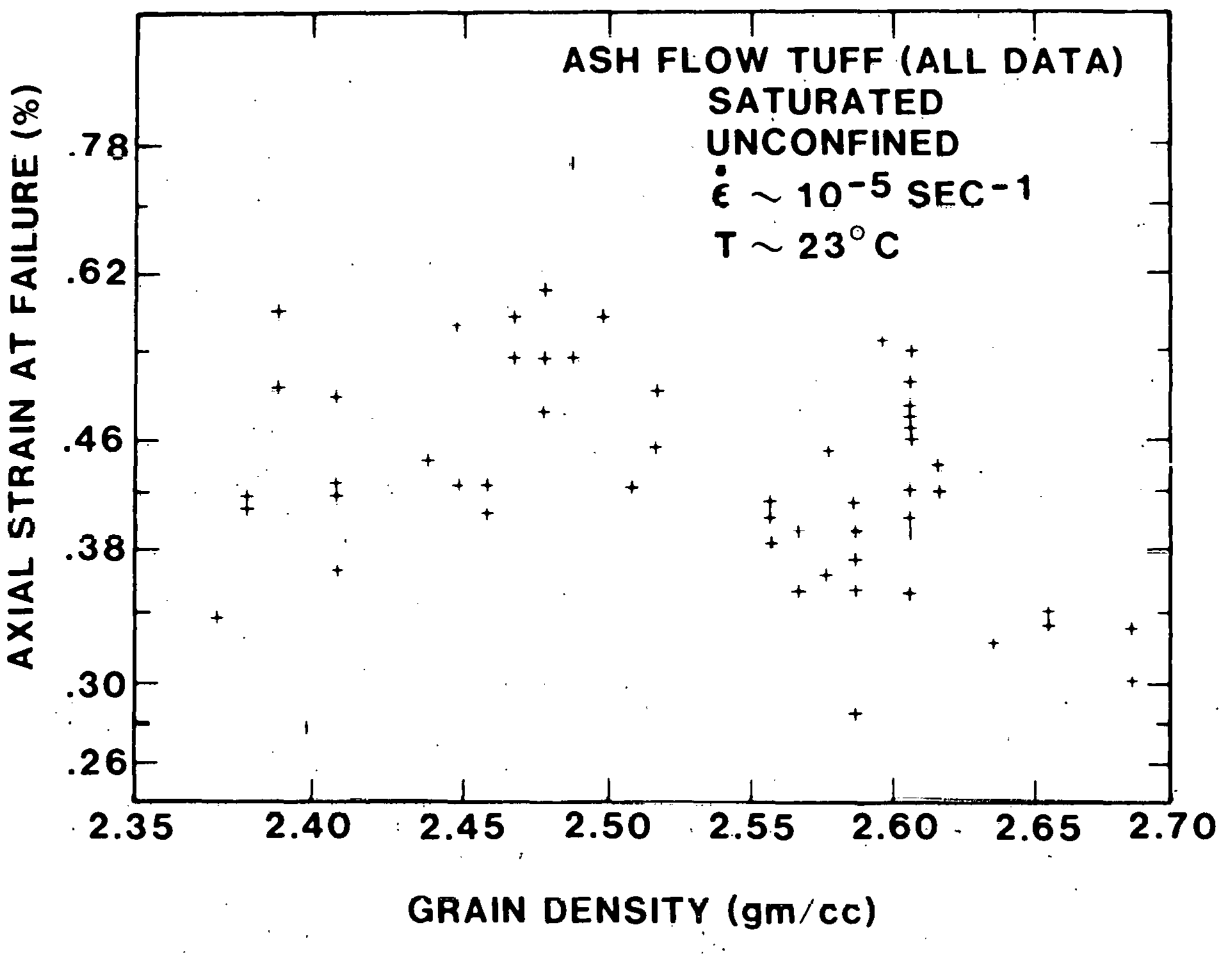

Figure 12

A plot of axial strain at failure as a function of grain density for SNLA data from the Calico Hills, Bullfrog and Tram ash flow tuffs. All tests were run on saturated samples under unconfined, room temperature and 10^{-5} s^{-1} conditions.

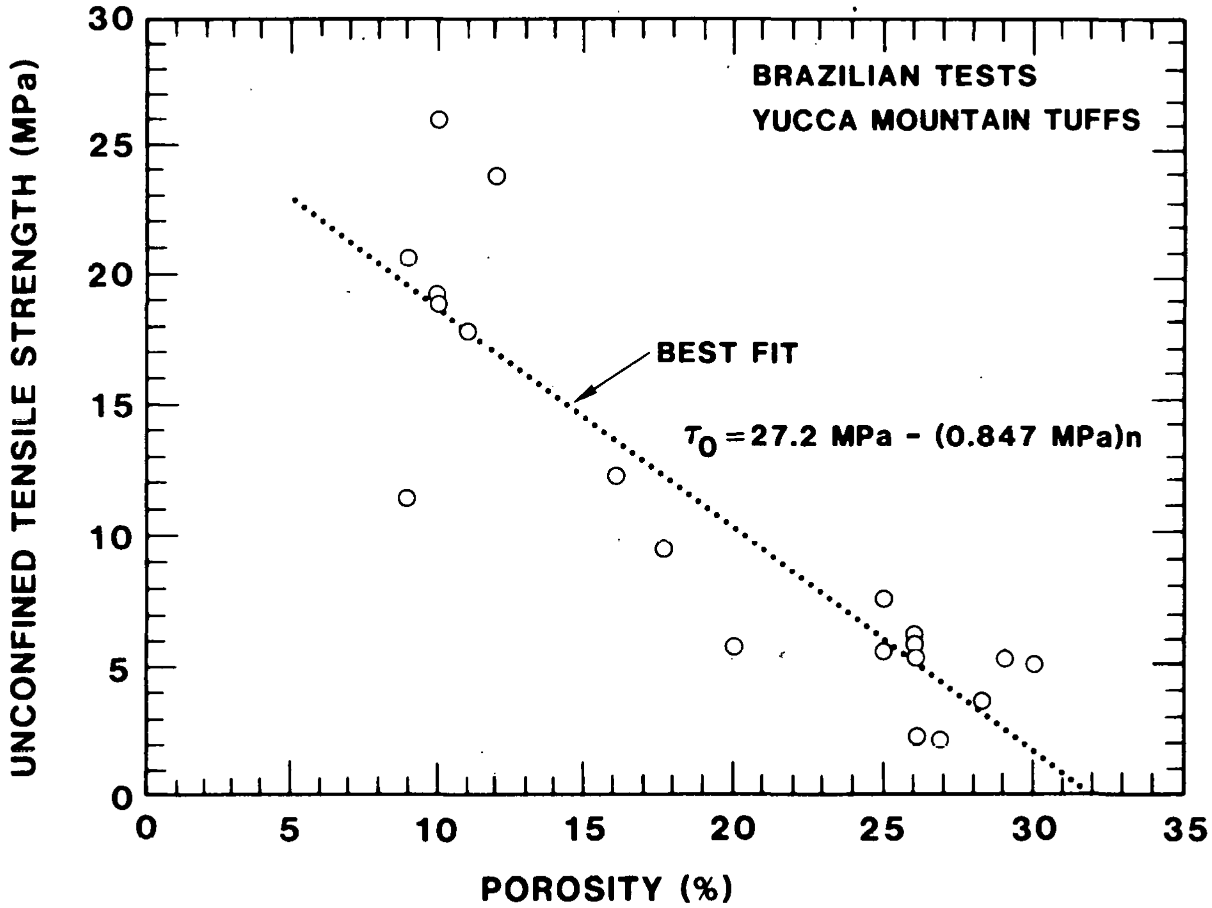

Figure 13

A plot of unconfined tensile strength as a function of effective porosity. All data were obtained from Brazilian (indirect-tensile) tests. (Data from Reference 1).

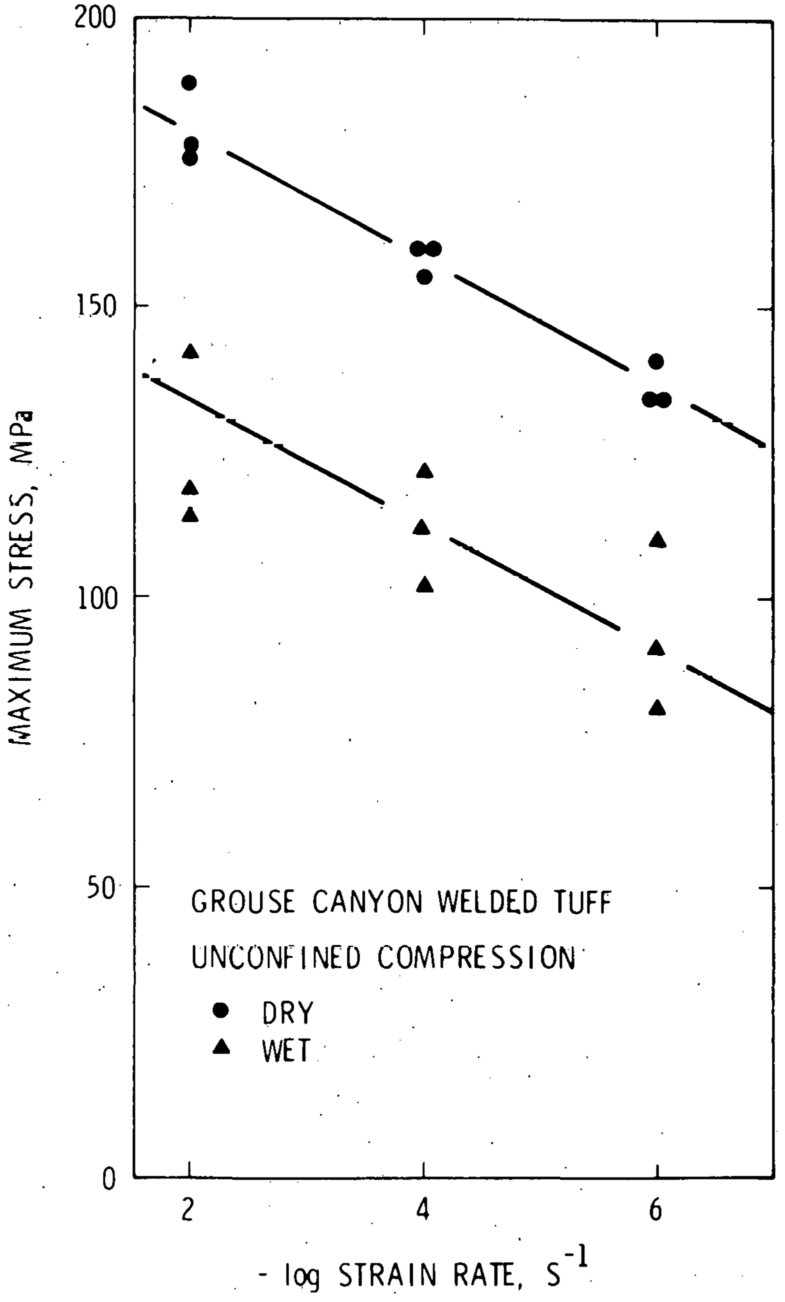

Figure 14

A plot of maximum (ultimate) stress (strength) as a function of negative log strain rate for Grouse Canyon tuff data. The tests were run on dry (oven dried) and wet (saturated) samples under unconfined and room temperature conditions. (Figure from Reference 10.)

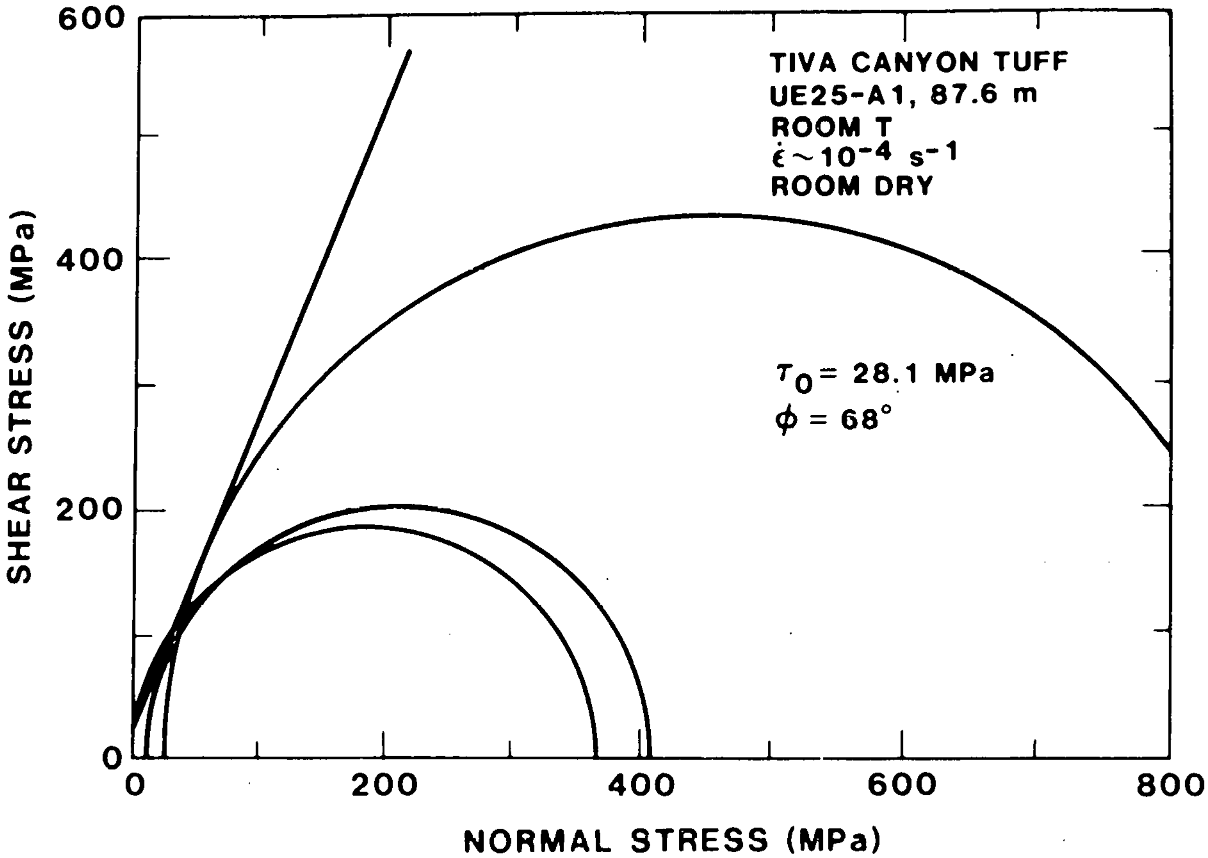

Figure 15A

Mohr-Coulomb plot of shear stress as a function of normal stress for Tiva Canyon Tuff samples from a depth of 87.6 m in drillhole UE25-A1. The experimental conditions and the Coulomb failure criteria fit parameters are noted on the figure.

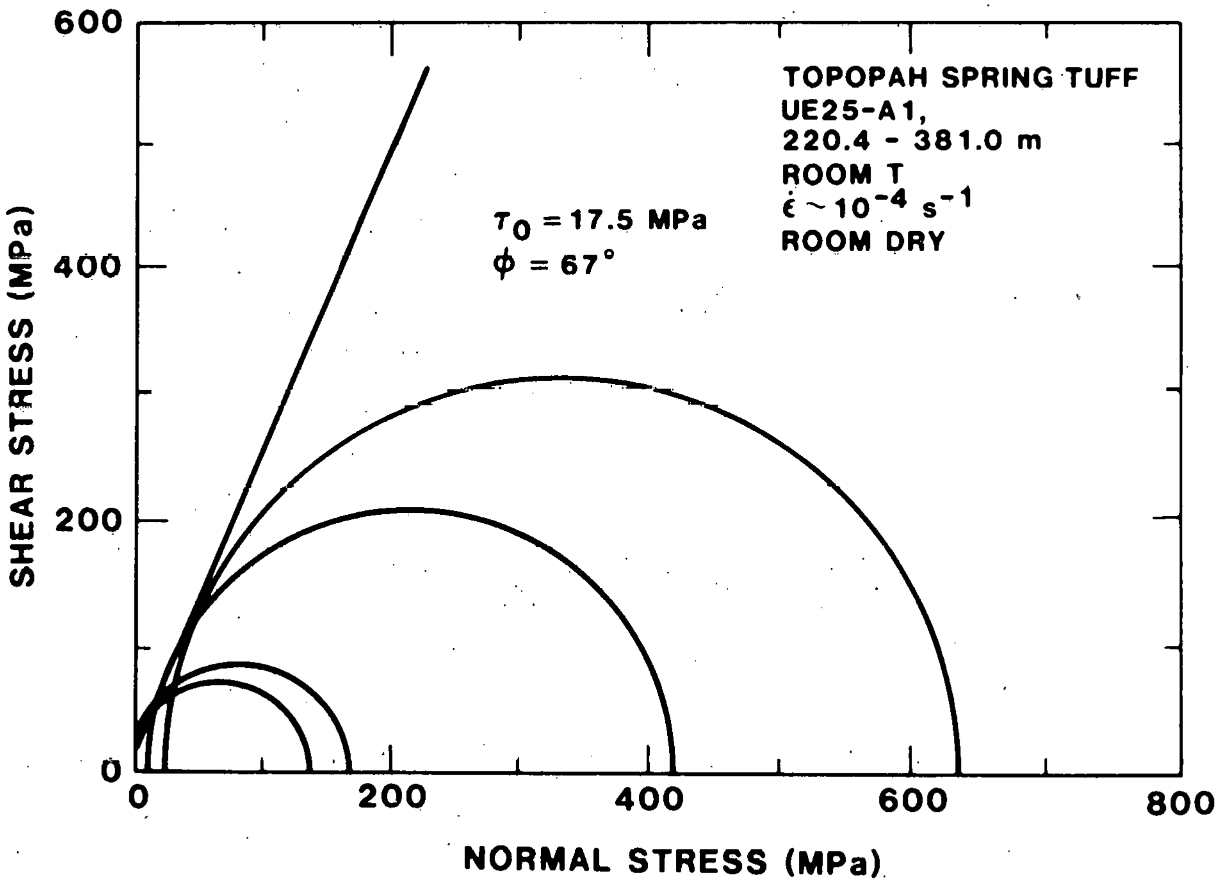

Figure 15B

Mohr-Coulomb plot of shear stress as a function of normal stress for Topopah Spring Tuff samples from depths of 220.4-381.0 m in drillhole UE25-A1. The experimental conditions and the Coulomb failure criteria fit parameters are noted on the figure.

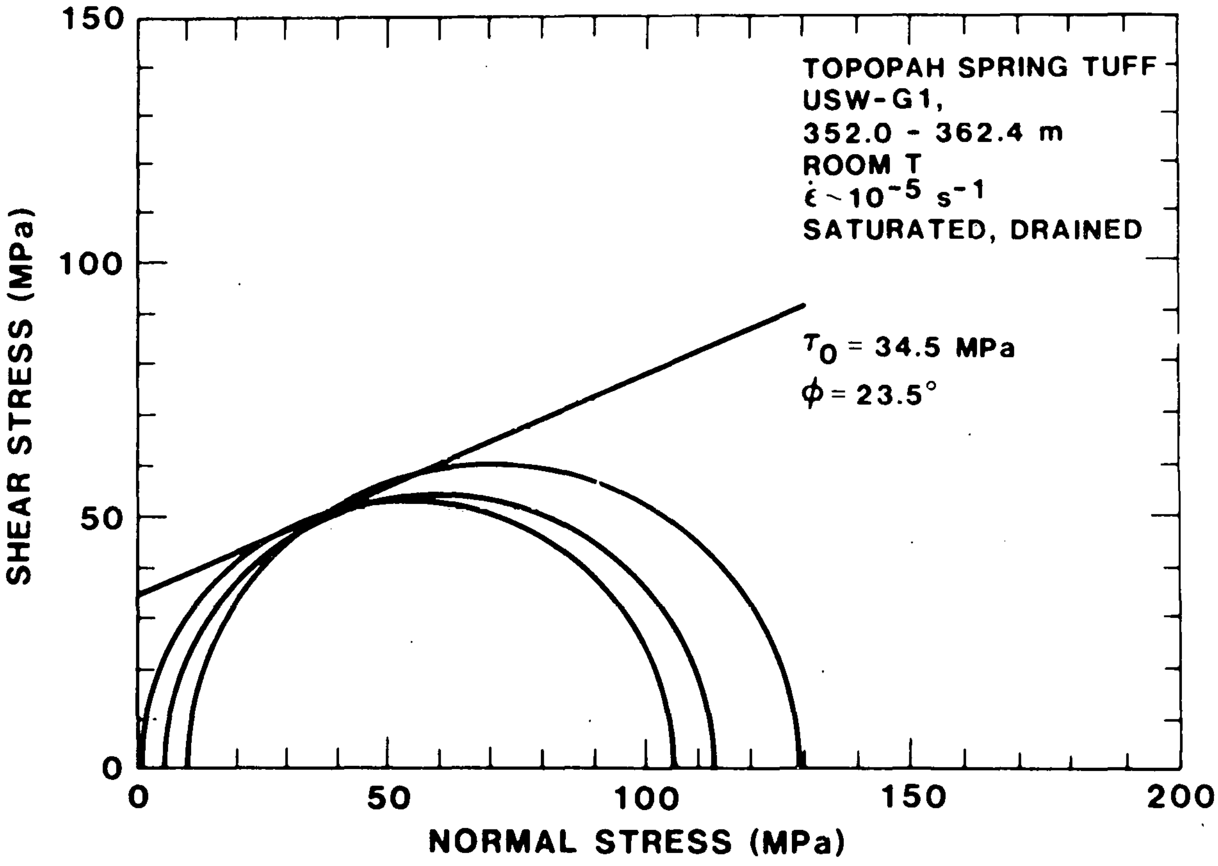

Figure 15C

Mohr-Coulomb plot of shear stress as a function of normal stress for Topopah Spring Tuff samples from depths of 352.0-362.4 m in drillhole USW-G1. The experimental conditions and the Coulomb failure criteria fit parameters are noted on the figure.

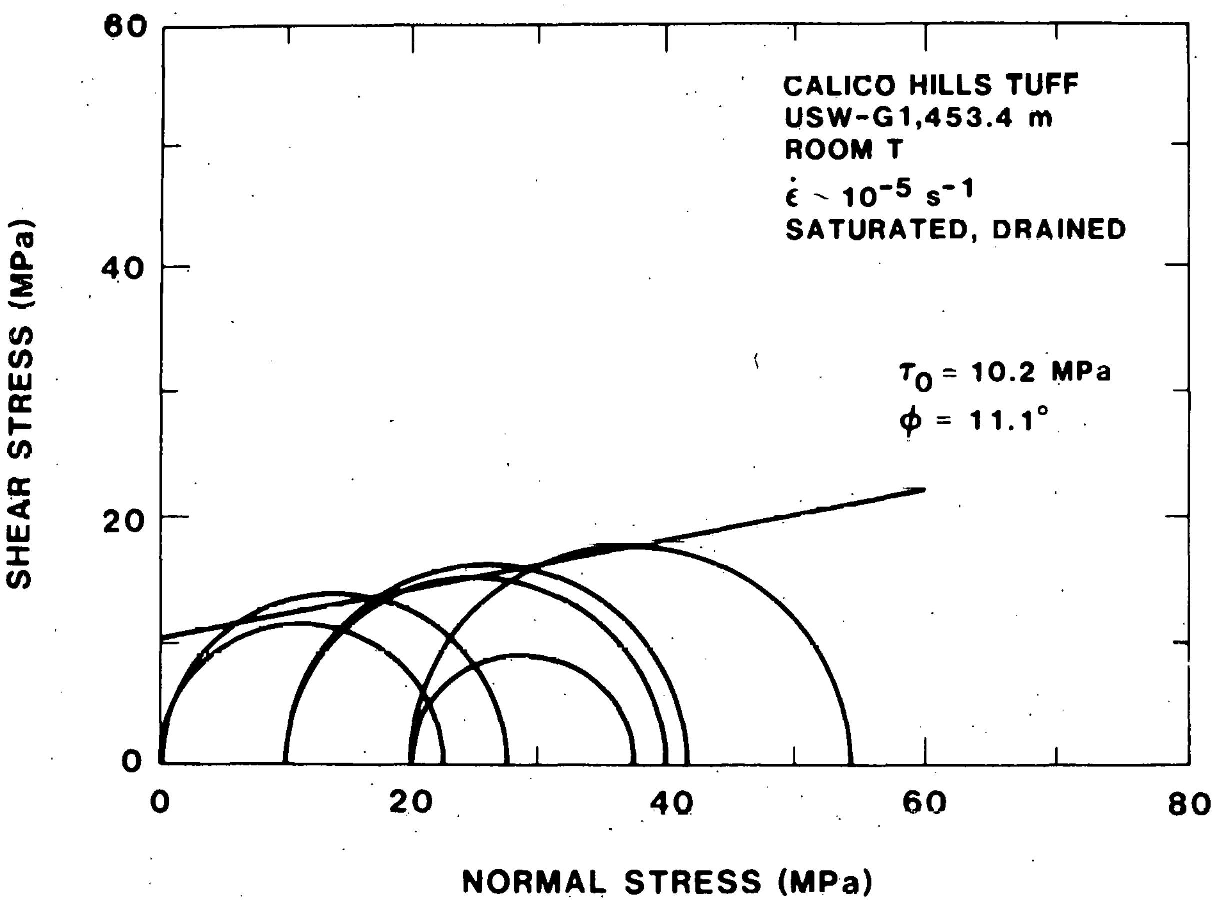

Figure 15D

Mohr-Coulomb plot of shear stress as a function of normal stress for Calico Hills Tuff samples from a depth of 453.4 m in drillhole USW-G1. The experimental conditions and the Coulomb failure criteria fit parameters are noted on the figure.

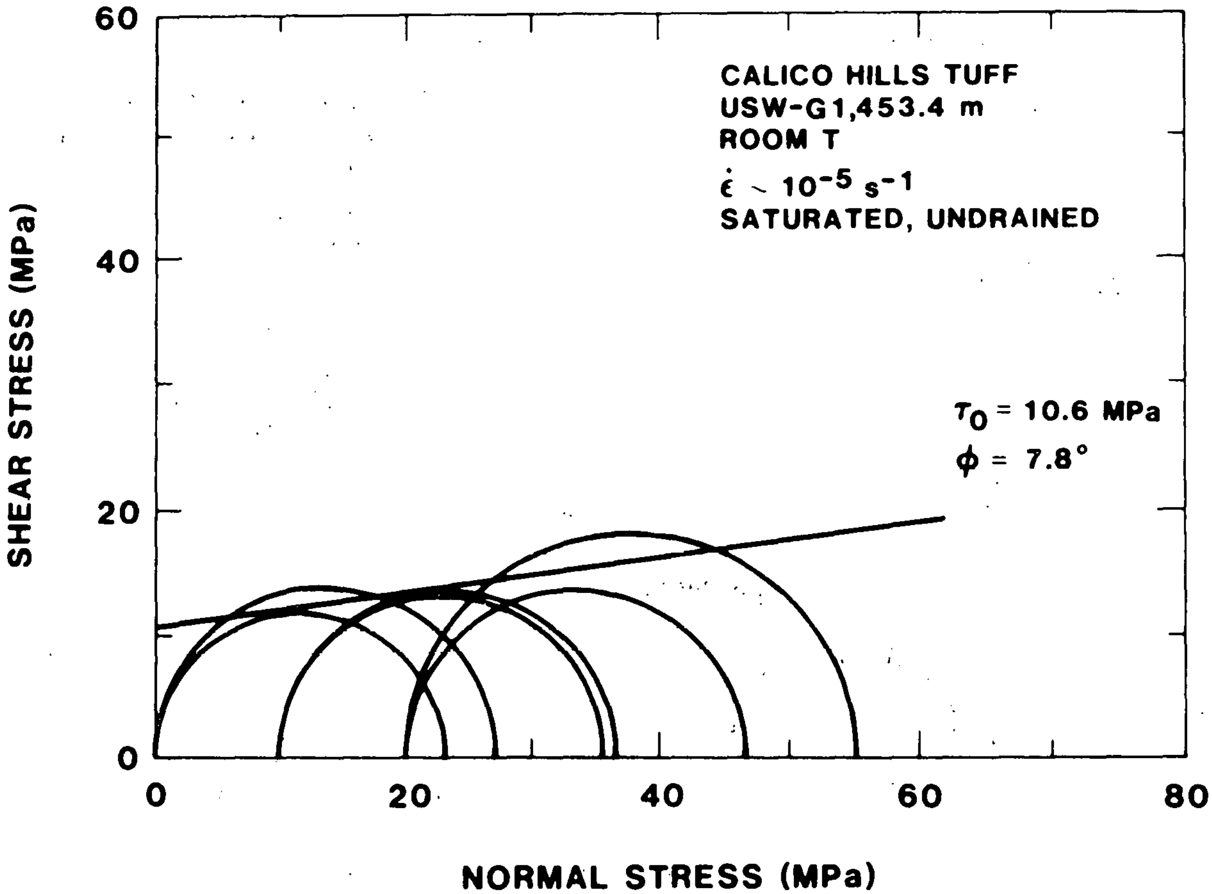

Figure 15E

Mohr-Coulomb plot of shear stress as a function of normal stress for Calico Hills Tuff samples from a depth of 453.4 m in drillhole USW-G1. The experimental conditions and the Coulomb failure criteria fit parameters are noted on the figure.

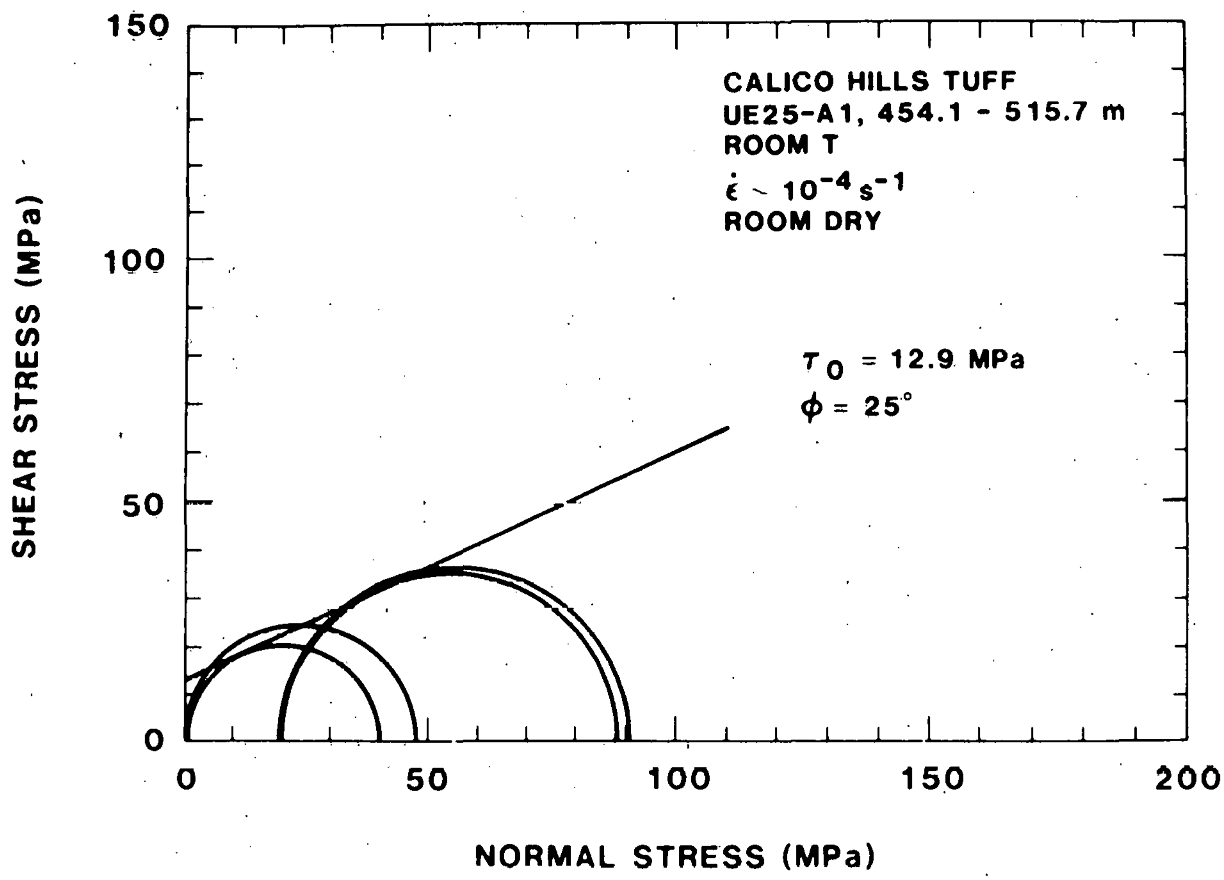

Figure 15F

Mohr-Coulomb plot of shear stress as a function of normal stress for Calico Hills Tuff samples from depths of 454.1-515.7 m in drillhole UE25-A1. The experimental conditions and the Coulomb failure criteria fit parameters are noted on the figure.

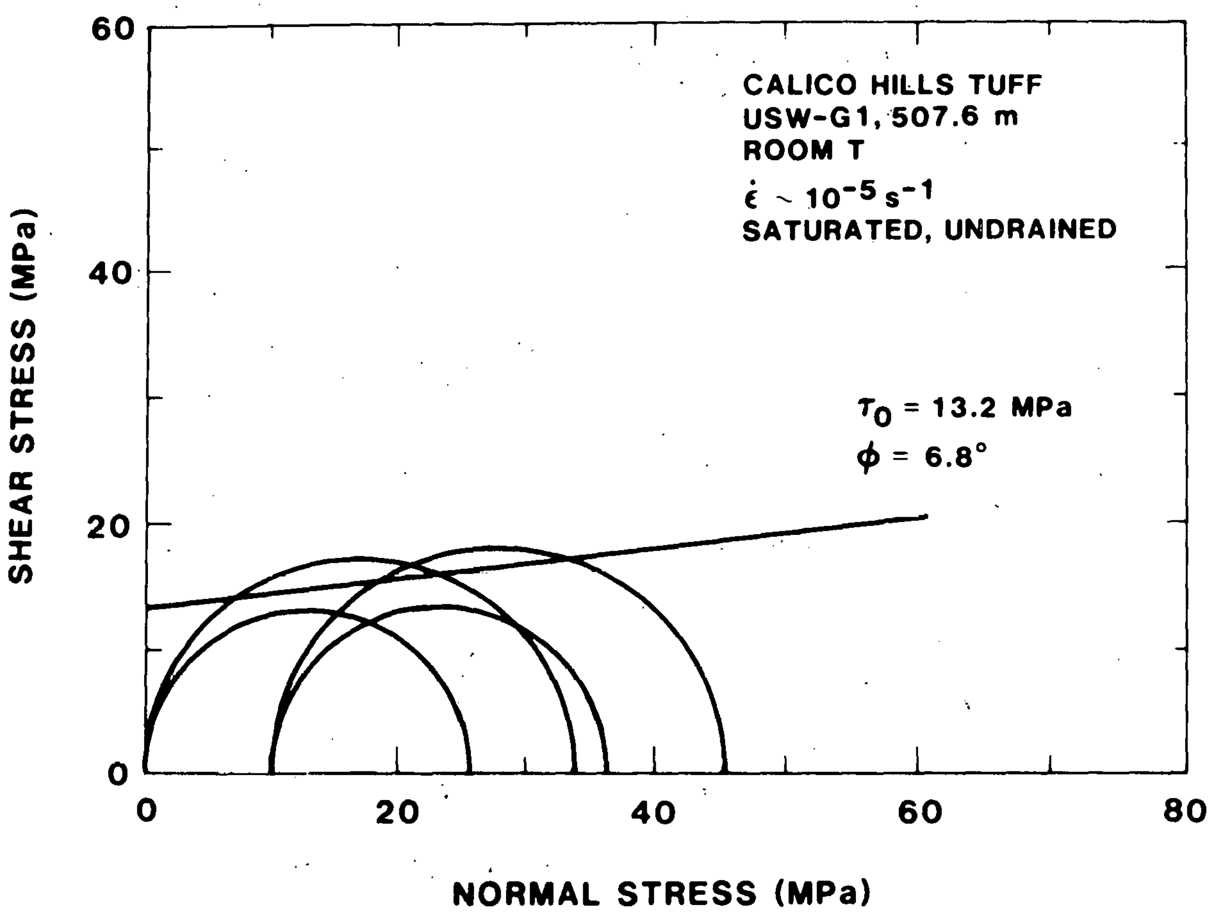

Figure 15G

Mohr-Coulomb plot of shear stress as a function of normal stress for Calico Hills Tuff samples from a depth of 507.6 m in drillhole USW-G1. The experimental conditions and the Coulomb failure criteria fit parameters are noted on the figure.

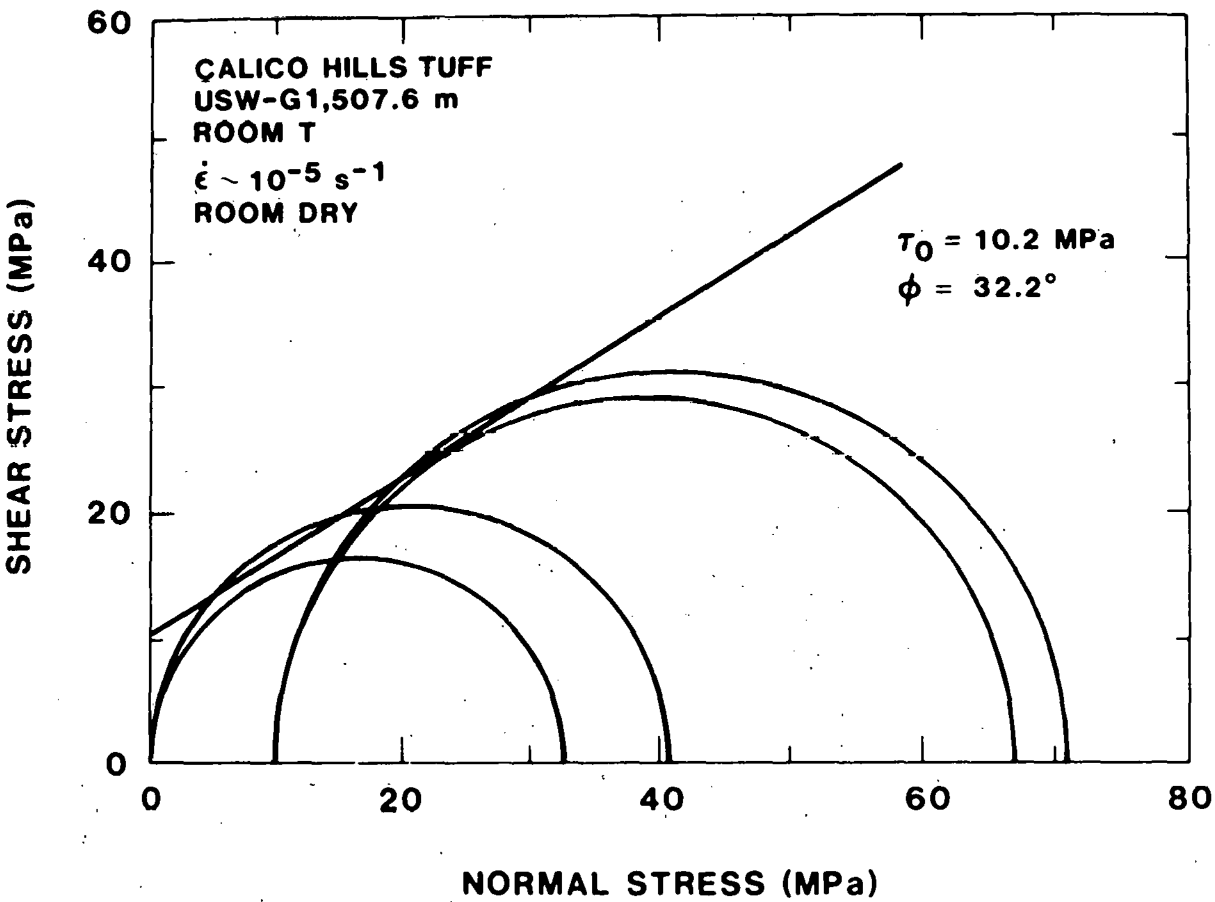

Figure 15H

Mohr-Coulomb plot of shear stress as a function of normal stress for Calico Hills Tuff samples from a depth of 507.6 m in drillhole USW-G1. The experimental conditions and the Coulomb failure criteria fit parameters are noted on the figure.

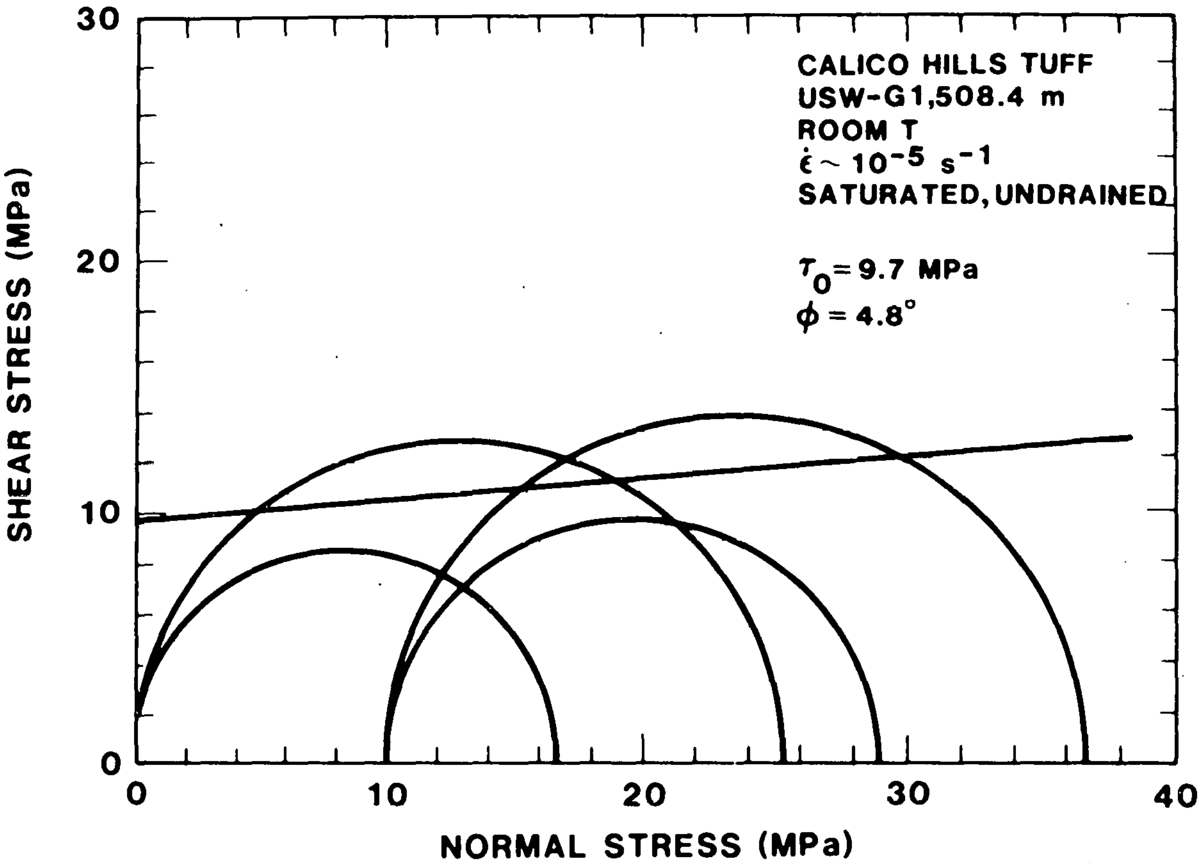

Figure 15I

Mohr-Coulomb plot of shear stress as a function of normal stress for Calico Hills Tuff samples from a depth of 508.4 m in drillhole USW-G1. The experimental conditions and the Coulomb failure criteria fit parameters are noted on the figure.

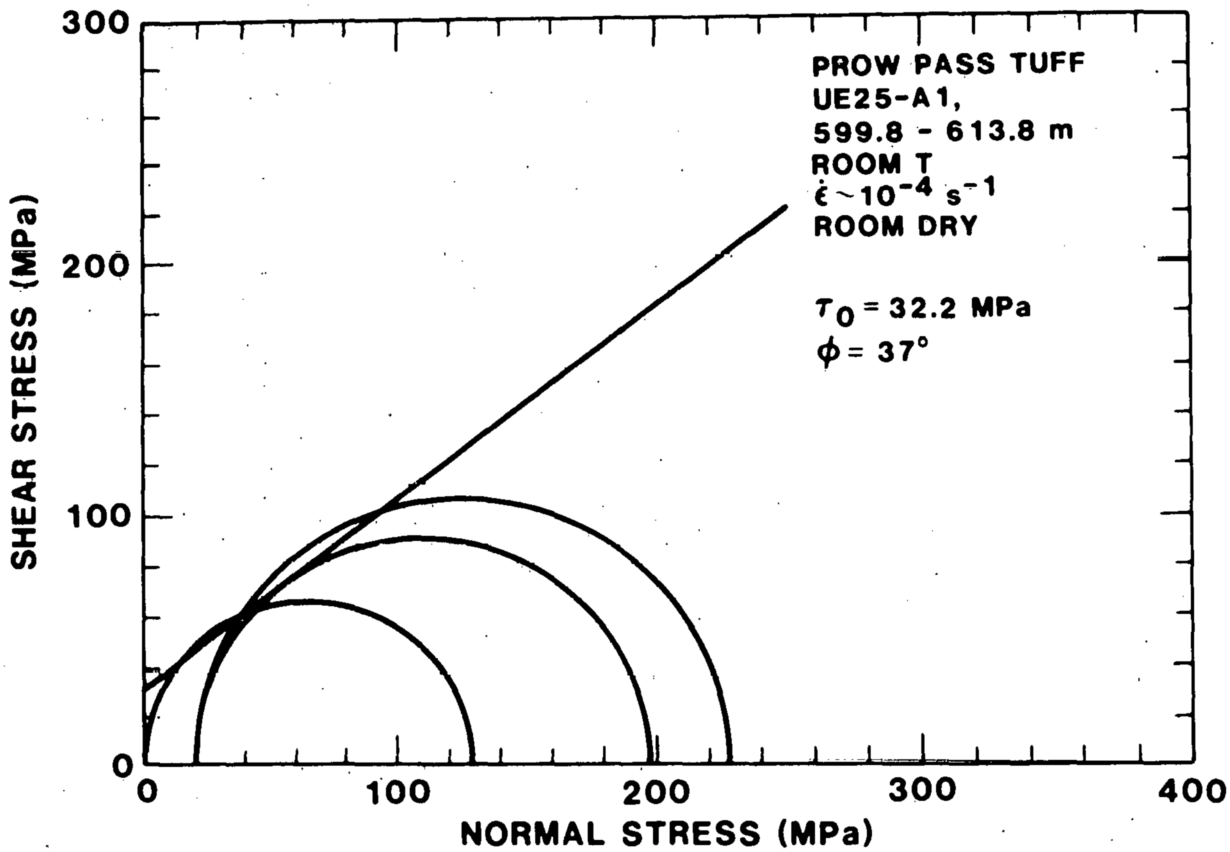

Figure 15J

Mohr-Coulomb plot of shear stress as a function of normal stress for Prow Pass Tuff samples from depths of 599.8-613.8 m in drillhole UE25-A1. The experimental conditions and the Coulomb failure criteria fit parameters are noted on the figure.

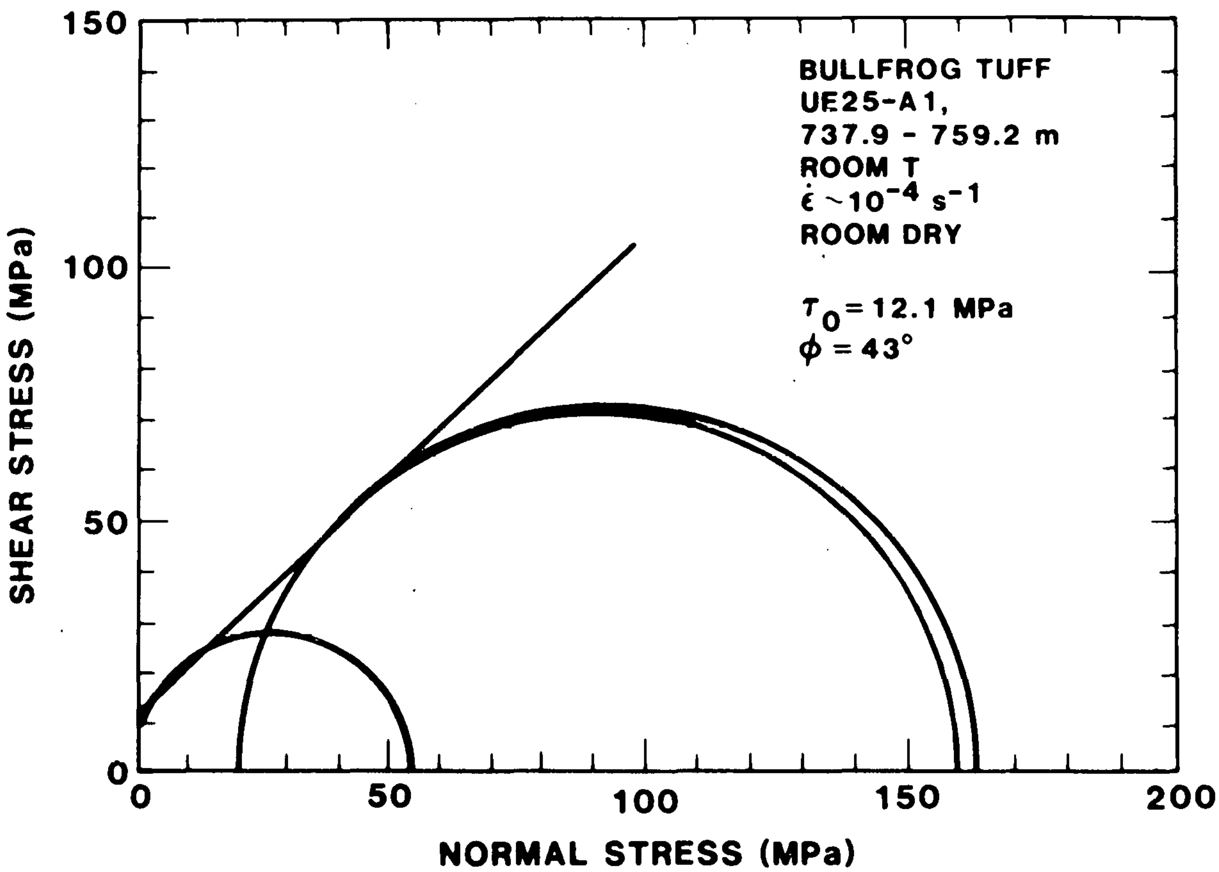

Figure 15K

Mohr-Coulomb plot of shear stress as a function of normal stress for Bullfrog Tuff samples from depths of 737.9-759.2 m in drillhole UE25-A1. The experimental conditions and the Coulomb failure criteria fit parameters are noted on the figure.

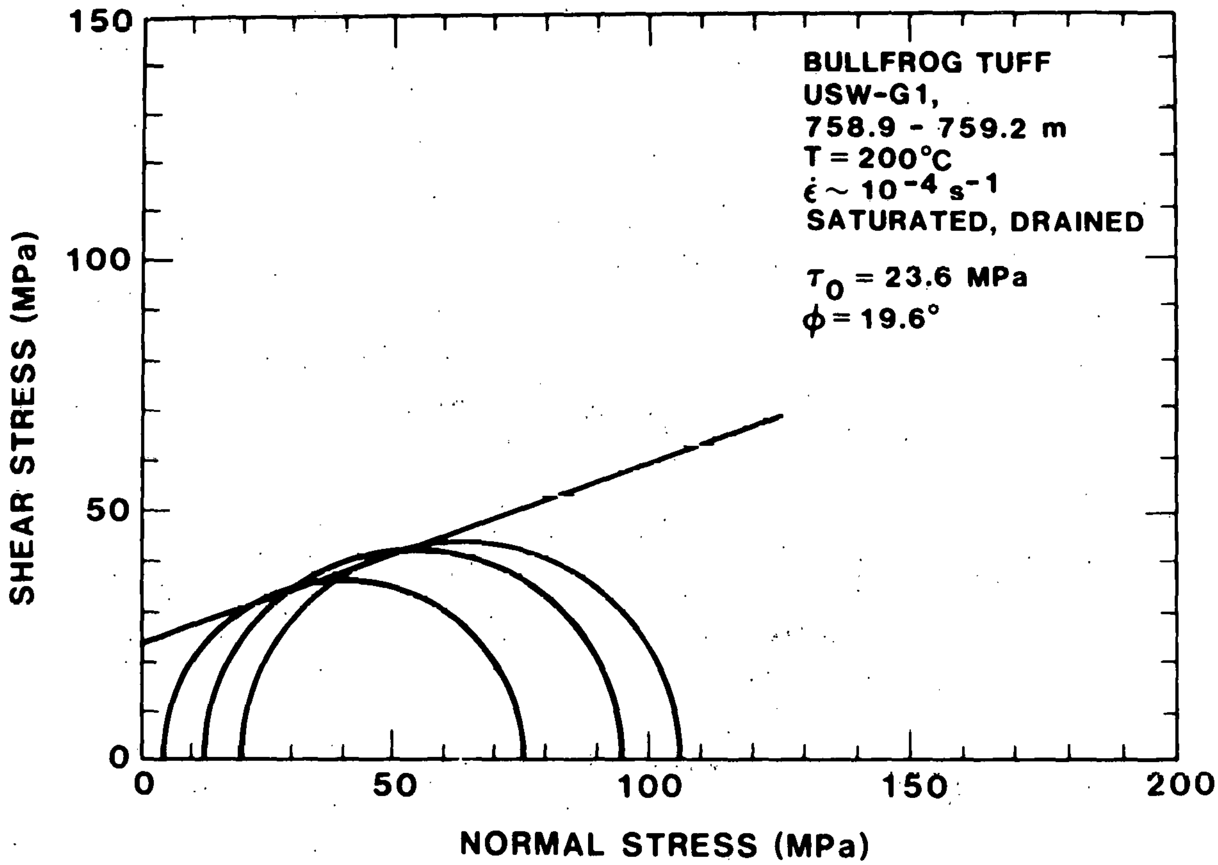

Figure 15L

Mohr-Coulomb plot of shear stress as a function of normal stress for Bullfrog Tuff samples from depths of 758.9-759.2 m in drillhole USW-G1. The experimental conditions and the Coulomb failure criteria fit parameters are noted on the figure.

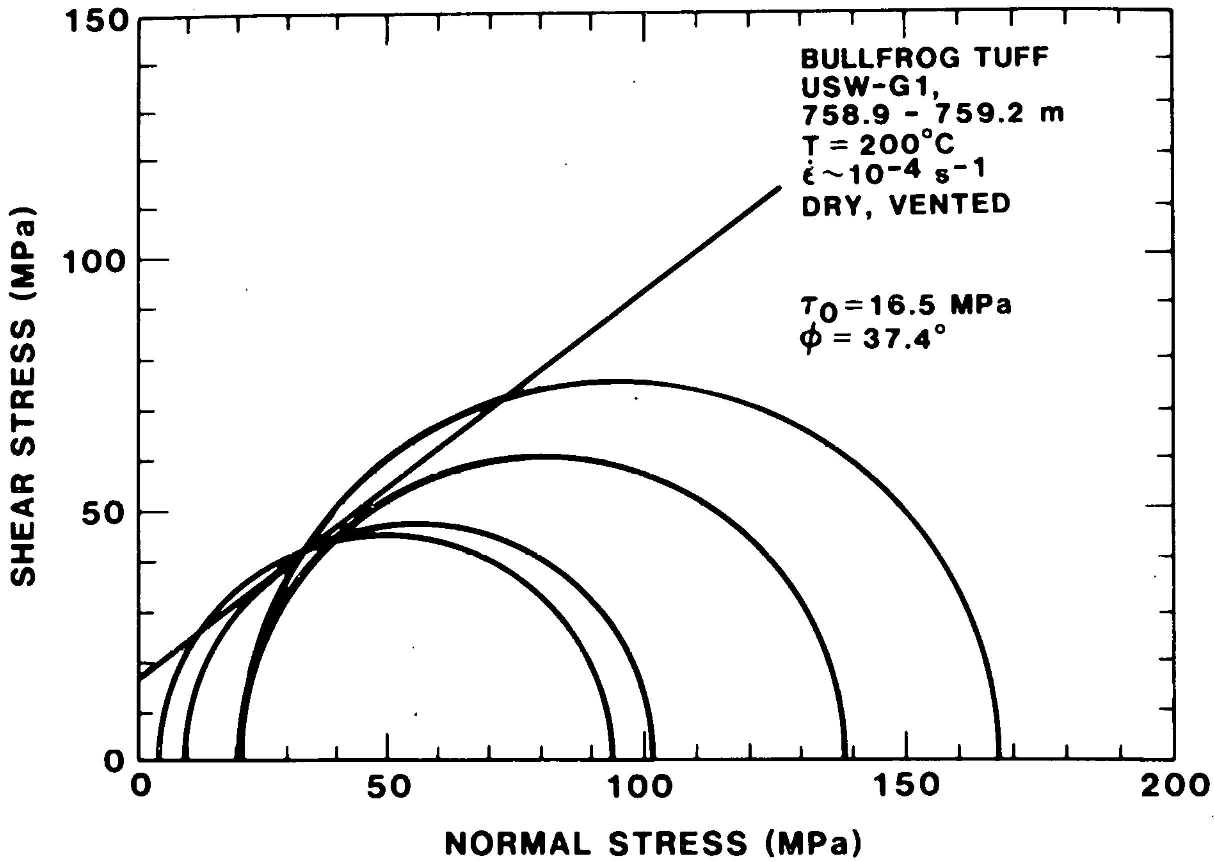

Figure 15M

Mohr-Coulomb plot of shear stress as a function of normal stress for Bullfrog Tuff samples from depths of 758.9-759.2 m in drillhole USW-G1. The experimental conditions and the Coulomb failure criteria fit parameters are noted on the figure.

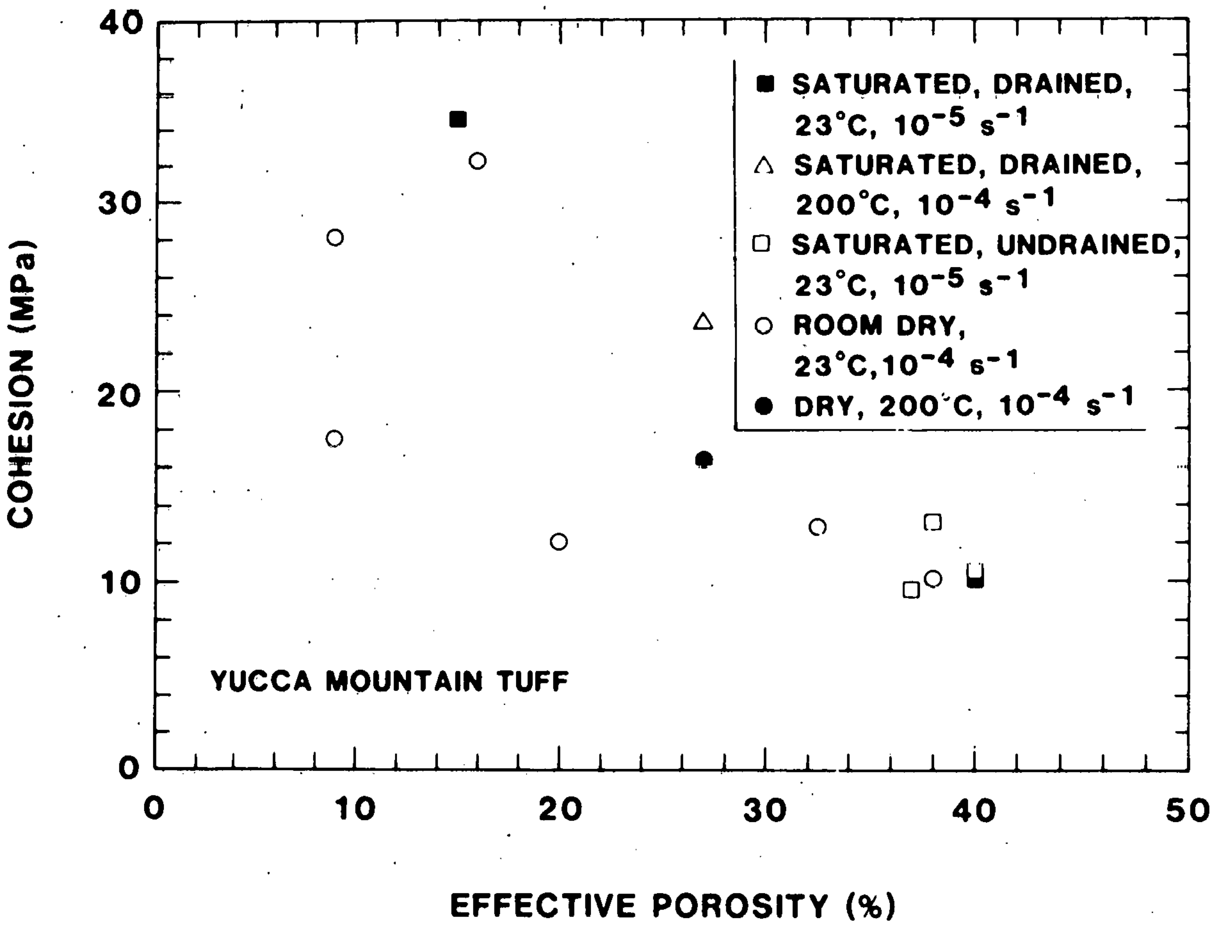

Figure 16

A plot of cohesion as a function of effective porosity for all pressure-effects test series on Yucca Mountain tuff samples. The experimental conditions for each data point are noted on the figure.

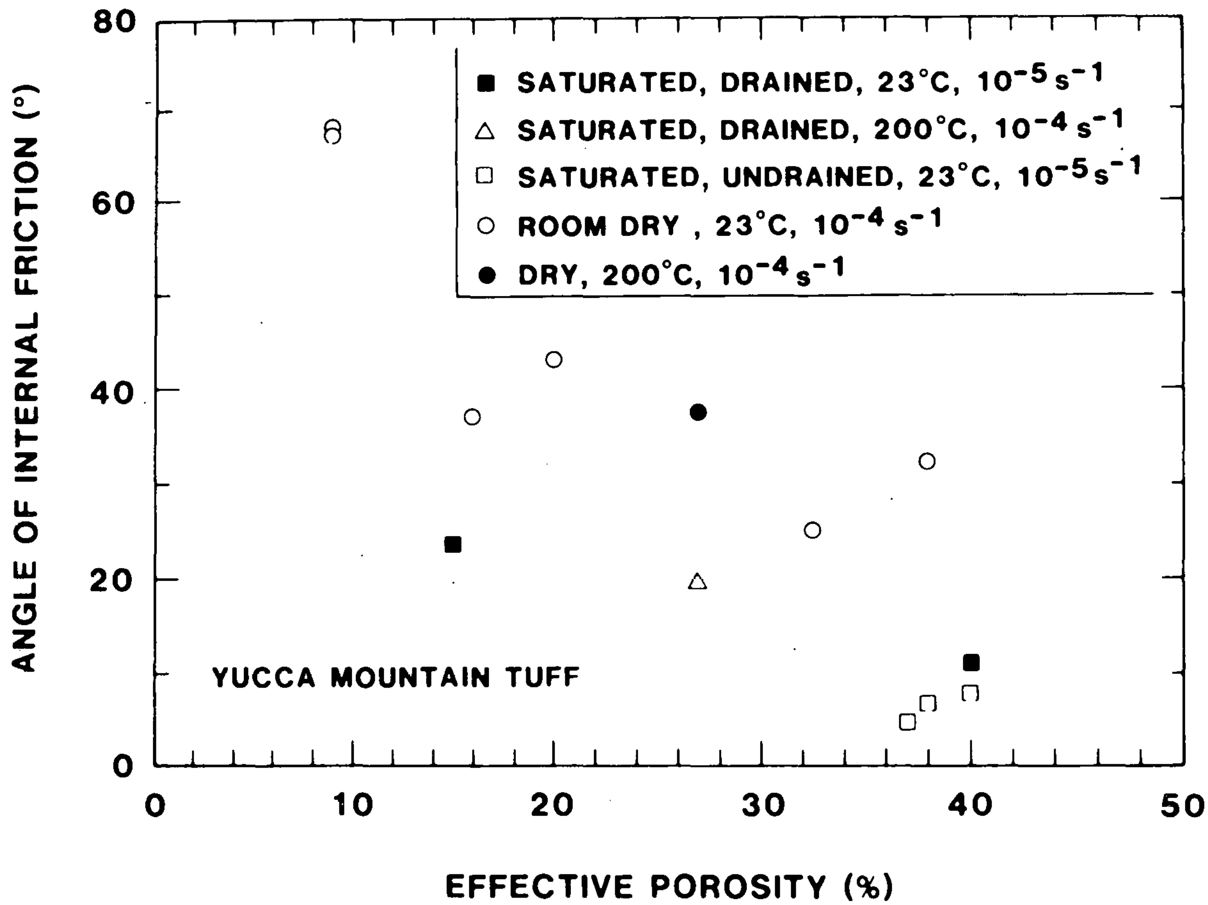

Figure 17

A plot of angle of internal friction as a function of effective porosity for all pressure-effects test series on Yucca Mountain tuff samples. The experimental conditions for each data point are noted on the figure.

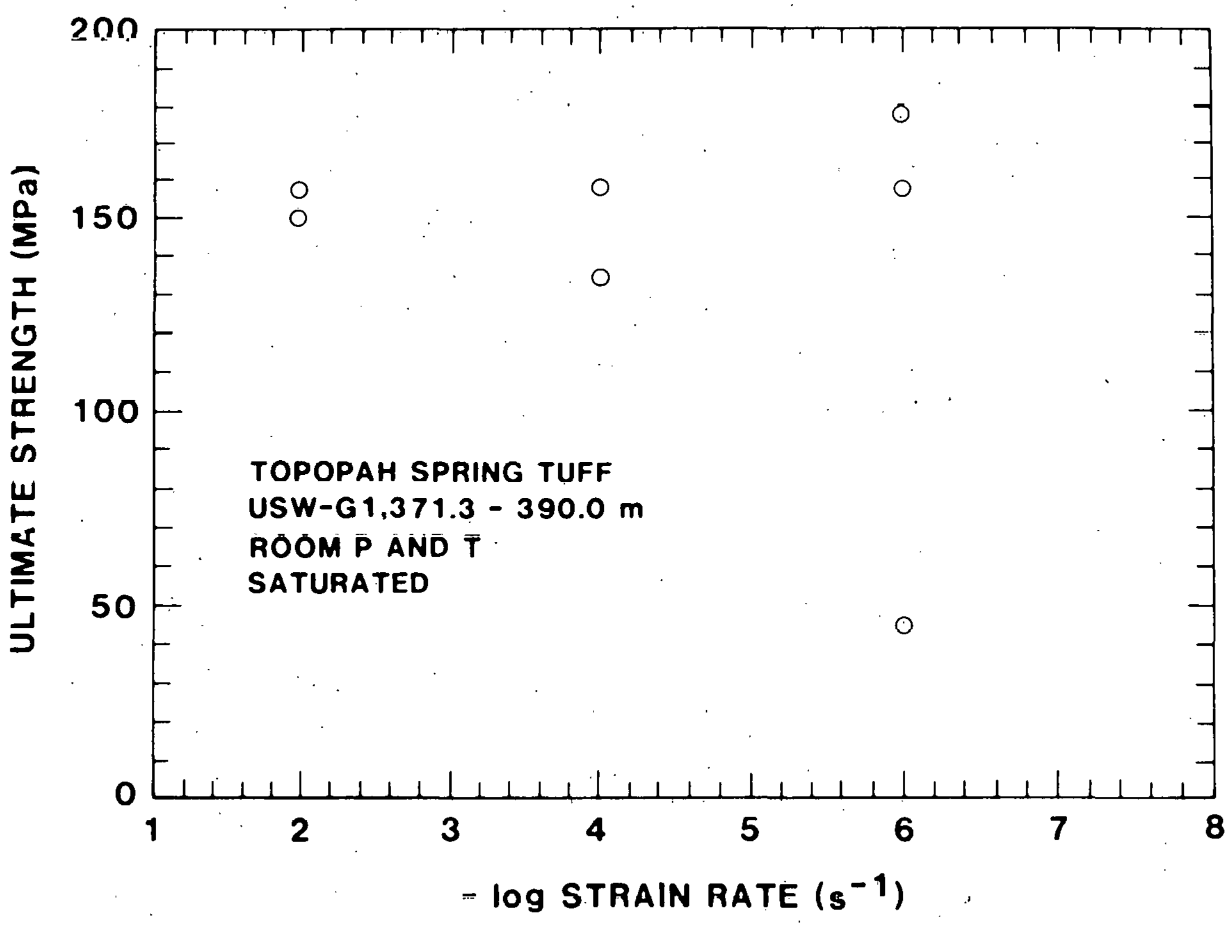

Figure 18A

Plot of ultimate strength as a function of negative log strain rate for Topopah Spring Tuff test series. All tests were run on saturated samples under unconfined and room temperature conditions.

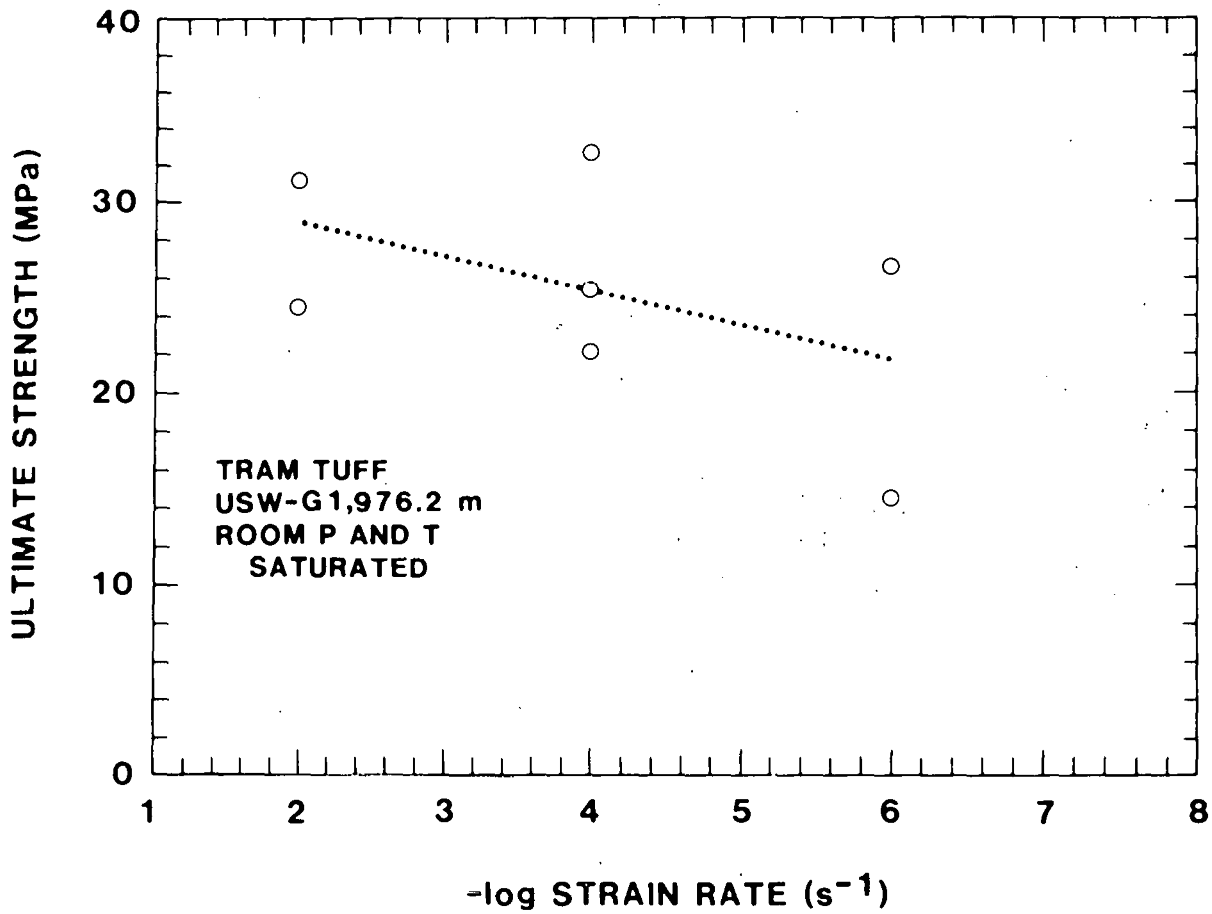

Figure 18B

Plot of ultimate strength as a function of negative log strain rate for Calico Hills Tuff test series. All tests were run on saturated samples under unconfined and room temperature conditions.

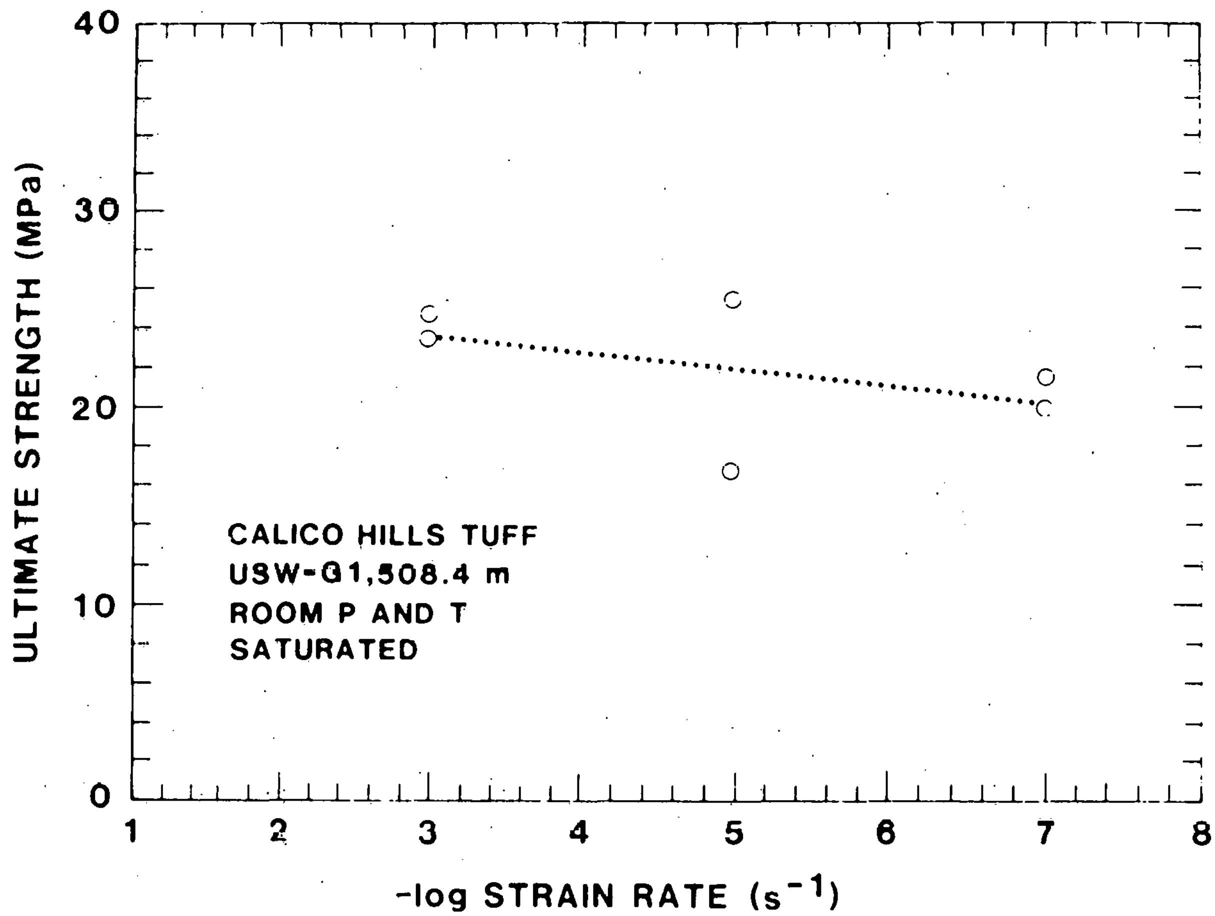

Figure 18C

Plot of ultimate strength as a function of negative log strain rate for Tram Tuff test series. All tests were run on saturated samples under unconfined and room temperature conditions.

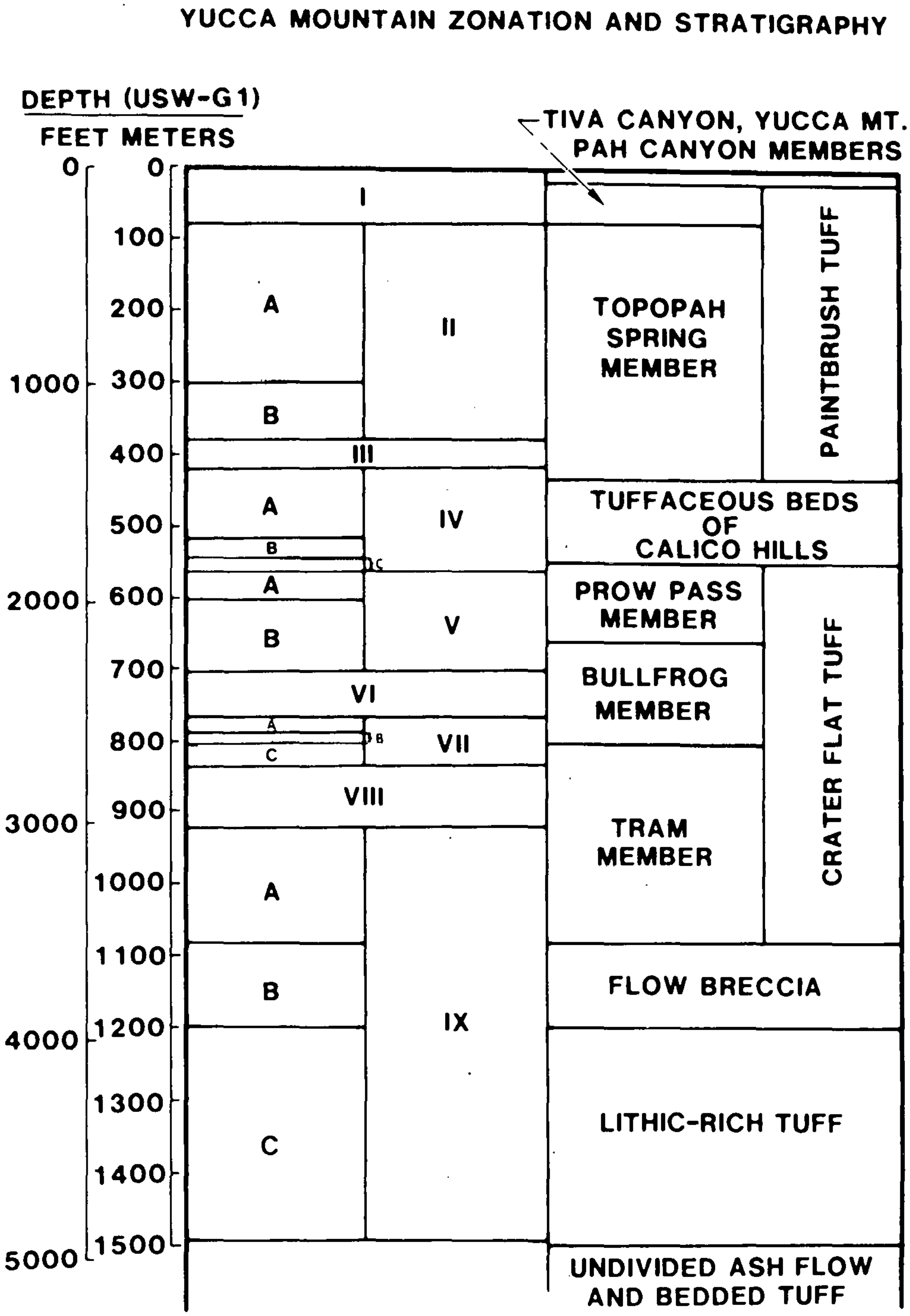

Figure 19

Yucca Mountain thermal/mechanical zonation correlated with drillhole USW-G1 stratigraphy.

Appendix

Unit	Depth (m)	P_c (MPa)	P_p (MPa)	P_e (MPa)	T (°C)	$\dot{\epsilon}$ (s^{-1})	S (Y,R,N)	D (Y,N)	$(\Delta\sigma)_u$ (MPa)	$(\epsilon_1)_u$ (%)	E (GPa)	ν	~n (%)	~ ρ_g (Mg/m^3)	Ref
TC	26.7 (A1)	0	0	0	23	10^{-4}	R	Y	364	-	57.5	.31	9	-	10
TC	26.7 (A1)	10	0	10	23	10^{-4}	R	Y	396	-	43.9	.30	9	-	10
TC	26.7 (A1)	20	0	20	23	10^{-4}	R	Y	875	-	58.3	.22	9	-	10
TC	56.4 (A1)	20.7	0	20.7	200	10^{-4}	R	Y	105	-	-	-	27	-	10
TC	64.8 (A1)	0	0	0	23	10^{-4}	R	Y	7.03	-	41	.28	54	-	10
TS	220.4 (A1)	0	0	0	23	10^{-4}	R	Y	138	-	40.4	.22	13	-	10
TS	225.4 (A1)	20.7	0	20.7	200	10^{-4}	R	Y	133	-	23.9	.15	11	-	10
TS	311.4 (G1)	0	0	0	23	10^{-5}	Y	Y	75.2	.38	25.5	.25	-	-	16
TS	323.3 (G1)	0	0	0	23	10^{-5}	Y	Y	142.8	.50	38.1	.32	-	-	16
TS	334.0 (G1)	0	0	0	23	10^{-5}	Y	Y	59.8	.34	24.9	.15	-	-	16
TS	352.0 (G1)	0	0	0	23	10^{-5}	Y	Y	106.2	.37	32.5	.33	-	-	16
TS	352.0 (G1)	5	0	5	23	10^{-5}	Y	N	72.5	.59	19.2	.14	-	-	16
TS	354.6 (G1)	5	0	5	23	10^{-5}	Y	N	219.3	.74	35.6	.30	-	-	16
TS	359.5 (G1)	5	0	5	23	10^{-5}	Y	Y	109.7	.69	23.2	.32	-	-	16
TS	362.4 (G1)	10	0	10	23	10^{-5}	Y	Y	119.3	.66	25.6	.30	-	-	16
TS	371.3 (G1)	0	0	0	23	10^{-6}	Y	Y	176.6	.51	40.8	.25	-	-	16
TS	372.5 (G1)	0	0	0	23	10^{-2}	Y	Y	157.2	.48	29.2	.31	-	-	16
TS	372.5 (G1)	0	0	0	23	10^{-4}	Y	Y	133.8	.57	27.7	.34	-	-	16
TS	373.0 (G1)	0	0	0	23	10^{-4}	Y	Y	157.2	.46	37.5	.25	-	-	16
TS	373.0 (G1)	0	0	0	23	10^{-6}	Y	Y	156.6	.47	35.3	.21	-	-	16

Appendix - Continued

Unit	Depth (m)	P_c (MPa)	P_p (MPa)	P_e (MPa)	T (°C)	$\dot{\epsilon}$ (s^{-1})	S (Y,R,N)	D (Y,N)	$(\Delta\sigma)_u$ (MPa)	$(\epsilon_1)_u$ (%)	E (GPa)	ν	~n (%)	~ ρ_g (Mg/m^3)	Ref
TS	381.0 (A1)	0	0	0	23	10^{-4}	R	Y	166	-	61.8	.30	9	-	10
TS	381.0 (A1)	10	0	10	23	10^{-4}	R	Y	412	-	73.0	.23	9	-	10
TS	381.0 (A1)	20	0	20	23	10^{-4}	R	Y	618	-	59.9	.21	9	-	10
TS	384.8 (G1)	0	0	0	23	10^{-2}	Y	Y	149.7	.49	36.6	-	-	-	16
TS	390.0 (G1)	0	0	0	23	10^{-6}	Y	Y	44.9	.41	22.9	.27	-	-	16
CH	439.5 (G1)	0	0	0	23	10^{-5}	Y	Y	21.7	.43	6.40	-	39	2.51	15
CH	439.5 (G1)	0	0	0	23	10^{-5}	Y	Y	22.0	.43	5.79	-	39	2.51	15
CH	439.5 (G1)	0	0	0	23	10^{-5}	Y	Y	24.3	.43	6.03	.09	39	2.51	18
CH	439.5 (G1)	0	0	0	23	10^{-5}	Y	Y	34.2	.56	8.84	.07	39	2.51	18
CH	453.4 (G1)	0	0	0	23	10^{-5}	Y	Y	22.9	.58	4.87	-	40	2.50	15
CH	453.4 (G1)	0	0	0	23	10^{-5}	Y	Y	45.3	.62	9.42	.09	40	2.50	18
CH	453.4 (G1)	0	0	0	23	10^{-5}	Y	Y	23.2	.69	5.45	.09	40	2.50	18
CH	453.4 (G1)	10	0	10	23	10^{-5}	Y	N	25.4	.45	6.85	.34	40	2.50	15
CH	453.4 (G1)	10	0	10	23	10^{-5}	Y	N	26.0	.41	7.79	.34	40	2.50	15
CH	453.4 (G1)	10	0	10	23	10^{-5}	Y	Y	29.9	.68	5.57	-	40	2.50	15
CH	453.4 (G1)	10	0	10	23	10^{-5}	Y	Y	31.4	.66	6.16	.22	40	2.50	15
CH	453.4 (G1)	20	0	20	23	10^{-5}	Y	N	26.7	.50	7.38	-	40	2.50	15
CH	453.4 (G1)	20	0	20	23	10^{-5}	Y	N	36.1	.52	7.93	-	40	2.50	15
CH	453.4 (G1)	20	0	20	23	10^{-5}	Y	Y	17.1	.71	3.92	.18	40	2.50	15
CH	453.4 (G1)	20	0	20	23	10^{-5}	Y	Y	34.4	.64	6.24	.17	40	2.50	15
CH	454.1 (A1)	0	0	0	23	10^{-4}	R	Y	47.7	-	12.3	.14	28	-	10
CH	463.3 (G1)	0	0	0	23	10^{-5}	Y	Y	18.9	.76	4.93	-	39	2.49	15
CH	463.3 (G1)	0	0	0	23	10^{-5}	Y	Y	20.7	.54	5.14	-	39	2.49	15
CH	463.3 (G1)	0	0	0	23	10^{-5}	Y	Y	22.6	.60	5.61	.10	39	2.49	18
CH	463.3 (G1)	0	0	0	23	10^{-5}	Y	Y	29.6	.60	4.41	.17	39	2.49	18

Appendix - Continued

Unit	Depth (m)	P_c (MPa)	P_p (MPa)	P_e (MPa)	T (°C)	$\dot{\epsilon}$ (s^{-1})	S (Y,R,N)	D (Y,N)	$(\Delta\sigma)_u$ (MPa)	$(\epsilon_1)_u$ (%)	E (GPa)	ν	~n (%)	~ ρ_g (Mg/m^3)	Ref
CH	472.6 (G1)	0	0	0	23	10^{-5}	Y	Y	35.9	.61	7.03	-	43	2.48	15
CH	472.6 (G1)	0	0	0	23	10^{-5}	Y	Y	30.5	.54	7.45	-	43	2.48	15
CH	472.6 (G1)	0	0	0	23	10^{-5}	Y	Y	53.1	.70	12.8	.07	43	2.48	18
CH	472.6 (G1)	0	0	0	23	10^{-5}	Y	Y	40.6	.64	9.12	.07	43	2.48	18
CH	486.1 (G1)	0	0	0	23	10^{-5}	Y	Y	14.2	.41	3.51	-	40	2.38	15
CH	486.1 (G1)	0	0	0	23	10^{-5}	Y	Y	15.3	.42	4.23	.19	40	2.38	15
CH	486.1 (G1)	0	0	0	23	10^{-5}	Y	Y	22.3	.43	6.37	.10	40	2.38	18
CH	486.1 (G1)	0	0	0	23	10^{-5}	Y	Y	22.3	.42	6.60	.09	40	2.38	18
CH	489.2 (A1)	20	0	20	23	10^{-4}	R	Y	26.1	-	7.99	.22	30	-	10
CH	492.9 (G1)	0	0	0	23	10^{-5}	Y	Y	26.5	.43	7.86	.26	37	2.41	15
CH	492.9 (G1)	0	0	0	23	10^{-5}	Y	Y	19.4	.37	7.17	.25	37	2.41	15
CH	492.9 (G1)	0	0	0	23	10^{-5}	Y	Y	42.7	.48	11.0	.10	37	2.41	18
CH	492.9 (G1)	0	0	0	23	10^{-5}	Y	Y	26.6	.36	9.41	.10	37	2.41	18
CH	498.0 (A1)	20.7	0	20.7	23	10^{-4}	R	Y	67.5	-	8.50	.27	32	-	10
CH	506.6 (A1)	20	0	20	23	10^{-4}	R	Y	70.3	-	9.57	.25	35	-	10
CH	507.6 (G1)	0	0	0	23	10^{-5}	Y	Y	26.2	.50	6.86	.18	38	2.41	15
CH	507.6 (G1)	0	0	0	23	10^{-5}	Y	Y	34.1	.42	9.52	-	38	2.41	15
CH	507.6 (G1)	0	0	0	23	10^{-5}	Y	Y	23.7	.57	6.39	.18	38	2.41	18
CH	507.6 (G1)	0	0	0	23	10^{-5}	Y	Y	37.6	.47	9.85	.14	38	2.41	18
CH	507.6 (G1)	0	0	0	23	10^{-5}	R	Y	41.0	.58	8.12	.29	38	2.41	15
CH	507.6 (G1)	0	0	0	23	10^{-5}	R	Y	32.7	.54	6.50	.31	38	2.41	15
CH	507.6 (G1)	10	0	10	23	10^{-5}	Y	N	35.7	.50	8.90	.31	38	2.41	15
CH	507.6 (G1)	10	0	10	23	10^{-5}	Y	N	27.6	.59	8.48	.30	38	2.41	15
CH	507.6 (G1)	10	0	10	23	10^{-5}	R	N	61.3	1.1	7.20	.27	38	2.41	15
CH	507.6 (G1)	10	0	10	23	10^{-5}	R	N	57.6	.99	7.34	.28	38	2.41	15
CH	507.6 (G1)	20	0	20	23	10^{-5}	Y	N	34.8	.54	9.31	-	38	2.41	15
CH	507.6 (G1)	20	0	20	23	10^{-5}	Y	N	36.2	.49	9.72	.25	38	2.41	15

Appendix - Continued

Unit	Depth (m)	P_c (MPa)	P_p (MPa)	P_e (MPa)	T (°C)	$\dot{\epsilon}$ (s^{-1})	S (Y,R,N)	D (Y,N)	$(\Delta\sigma)_u$ (MPa)	$(\epsilon_1)_u$ (%)	E (GPa)	ν	~n (%)	~ ρ_g (Mg/m^3)	Ref
CH	508.4 (G1)	0	0	0	23	10^{-3}	Y	Y	24.7	.61	5.41	.33	37	2.45	15
CH	508.4 (G1)	0	0	0	23	10^{-3}	Y	Y	23.4	.58	5.45	.49	37	2.45	15
CH	508.4 (G1)	0	0	0	23	10^{-5}	Y	Y	25.4	.57	6.15	.36	37	2.45	15
CH	508.4 (G1)	0	0	0	23	10^{-5}	Y	Y	16.7	.43	4.92	.18	37	2.45	15
CH	508.4 (G1)	10	0	10	23	10^{-5}	Y	N	18.9	.49	4.28	-	37	2.45	15
CH	508.4 (G1)	10	0	10	23	10^{-5}	Y	N	26.8	.57	6.01	.36	37	2.45	15
CH	508.4 (G1)	0	0	0	23	10^{-7}	Y	Y	21.5	.55	7.86	.21	37	2.45	15
CH	508.4 (G1)	0	0	0	23	10^{-7}	Y	Y	19.9	.51	7.03	.22	37	2.45	15
CH	515.7 (A1)	0	0	0	23	10^{-4}	R	Y	40.8	-	14.0	.20	37		10
CH	524.2 (G1)	0	0	0	23	10^{-5}	Y	Y	20.1	.43	5.83	.29	37	2.46	15
CH	524.2 (G1)	0	0	0	23	10^{-5}	Y	Y	27.4	.41	7.93	.30	37	2.46	15
CH	524.2 (G1)	0	0	0	23	10^{-5}	Y	Y	23.7	.50	6.81	.21	37	2.46	18
CH	524.2 (G1)	0	0	0	23	10^{-5}	Y	Y	34.6	.51	9.52	.10	37	2.46	18
CH	530.9 (G1)	0	0	0	23	10^{-5}	Y	Y	39.1	.87	8.41	.27	36	2.61	15
CH	530.9 (G1)	0	0	0	23	10^{-5}	Y	Y	42.0	.71	8.14	.32	36	2.61	15
CH	530.9 (G1)	0	0	0	23	10^{-5}	Y	Y	55.5	.63	12.4	.14	36	2.61	18
CH	530.9 (G1)	0	0	0	23	10^{-5}	Y	Y	70.7	.71	12.7	.15	36	2.61	18
CH	544.0 (G1)	0	0	0	23	10^{-5}	Y	Y	15.4	.79	2.55	.34	29	2.65	15
CH	544.0 (G1)	0	0	0	23	10^{-5}	Y	Y	14.8	.75	2.52	.37	29	2.65	15
CH	544.0 (G1)	0	0	0	23	10^{-5}	Y	Y	20.8	.73	4.05	.21	29	2.65	18
CH	544.0 (G1)	0	0	0	23	10^{-5}	Y	Y	21.6	.64	4.61	.20	29	2.65	18
PP	593.7 (A1)	100	0	100	23	10^{-4}	R	Y	299	-	22.0	.20	19	-	10
PP	599.8 (A1)	20	0	20	23	10^{-4}	R	Y	176	-	27.0	.20	18	-	10

Appendix - Continued

Unit	Depth (m)	P_c (MPa)	P_p (MPa)	P_e (MPa)	T (°C)	$\dot{\epsilon}$ (s^{-1})	S (Y,R,N)	D (Y,N)	$(\Delta\sigma)_u$ (MPa)	$(\epsilon_1)_u$ (%)	E (GPa)	ν	~n (%)	~ ρ_g (Mg/m^3)	Ref
PP	604.9 (G1)	0	0	0	23	10^{-5}	Y	Y	14.7	.36	4.91	.43	32	2.54	
PP	604.9 (G1)	0	0	0	23	10^{-5}	Y	Y	13.5	.30	5.25	.39	32	2.54	
PP	604.9 (G1)	0	0	0	23	10^{-5}	Y	Y	11.7	.35	3.14	.09	32	2.54	18
PP	604.9 (G1)	0	0	0	23	10^{-5}	Y	Y	13.6	.40	3.21	.05	32	2.54	18
PP	604.9 (A1)	20.7	0	20.7	23	10^{-4}	R	Y	207	-	31.0	.25	15	-	10
PP	613.8 (A1)	0	0	0	23	10^{-4}	R	Y	130	-	47.9	.30	17	-	10
PP	621.5 (A1)	0	0	0	23	10^{-4}	R	Y	32.2	-	7.84	.18	31	-	10
Bu	661.4 (G1)	0	0	0	23	10^{-5}	Y	Y	47.1	.49	11.5	.11	28	2.48	13
Bu	661.4 (G1)	0	0	0	23	10^{-5}	Y	Y	47.5	.46	8.58	.11	28	2.48	18
Bu	661.4 (G1)	0	0	0	23	10^{-5}	Y	Y	42.3	.46	8.67	.11	28	2.48	18
Bu	680.3 (G1)	0	0	0	23	10^{-5}	Y	Y	19.3	.45	5.34	.12	39	2.44	13
Bu	680.3 (G1)	0	0	0	23	10^{-5}	Y	Y	17.9	.52	2.76	.08	39	2.44	18
Bu	689.1 (G1)	0	0	0	23	10^{-5}	Y	Y	23.7	.40	6.24	.06	36	2.41	18
Bu	693.7 (G1)	0	0	0	23	10^{-5}	Y	Y	26.7	.28	10.3	.12	34	2.40	13
Bu	693.7 (G1)	0	0	0	23	10^{-5}	Y	Y	19.1	.54	2.72	.03	34	2.40	18
Bu	693.7 (G1)	0	0	0	23	10^{-5}	Y	Y	30.4	.58	3.73	.04	34	2.40	18
Bu	693.7 (G1)	0	0	0	23	10^{-5}	Y	Y	29.9	.46	5.76	.07	34	2.40	18
Bu	704.7 (G1)	0	0	0	23	10^{-5}	Y	Y	41.6	.34	15.8	.11	36	2.37	13
Bu	704.7 (G1)	0	0	0	23	10^{-5}	Y	Y	32.7	.35	9.56	.09	36	2.37	18
Bu	704.7 (G1)	0	0	0	23	10^{-5}	Y	Y	24.1	.34	8.17	.18	36	2.37	18
Bu	721.4 (G1)	0	0	0	23	10^{-5}	Y	Y	29.2	.50	8.38	.14	27	2.61	13
Bu	721.4 (G1)	0	0	0	23	10^{-5}	Y	Y	29.2	.50	8.38	.14	27	2.61	18
Bu	731.8 (A1)	50	0	50	23	10^{-4}	R	Y	174	-	18.7	.19	22	-	10

Appendix - Continued

Unit	Depth (m)	P_c (MPa)	P_p (MPa)	P_e (MPa)	T (°C)	$\dot{\epsilon}$ (s^{-1})	S (Y,R,N)	D (Y,N)	$(\Delta\sigma)_u$ (MPa)	$(\epsilon_1)_u$ (%)	E (GPa)	ν	~n (%)	~ ρ_g (Mg/m^3)	Ref
Bu	733.4 (G1)	0	0	0	23	10^{-5}	Y	Y	34.7	.41	9.82	-	25	2.56	8
Bu	733.4 (G1)	0	0	0	23	10^{-5}	Y	Y	35.8	.39	9.73	-	25	2.56	8
Bu	733.4 (G1)	0	0	0	23	10^{-5}	Y	Y	27	.50	7.74	.11	25	2.56	18
Bu	733.4 (G1)	0	0	0	23	10^{-5}	Y	Y	32	.53	8.89	.13	25	2.56	18
Bu	736.0 (G1)	0	0	0	23	10^{-5}	Y	Y	38.0	.42	10.2	-	28	2.59	8
Bu	736.0 (G1)	0	0	0	23	10^{-5}	Y	Y	36.0	.40	10.0	-	28	2.59	8
Bu	736.0 (G1)	0	0	0	23	10^{-5}	Y	Y	30.4	.38	8.10	-	28	2.59	8
Bu	736.0 (G1)	0	0	0	23	10^{-5}	Y	Y	35	.60	9.20	.12	28	2.59	18
Bu	736.0 (G1)	0	0	0	23	10^{-5}	Y	Y	36	.60	9.26	.13	28	2.59	18
Bu	736.0 (G1)	0	0	0	23	10^{-5}	Y	Y	29	.53	8.67	.16	28	2.59	18
Bu	737.9 (A1)	20	0	20	23	10^{-4}	R	Y	145	-	19.2	.23	22	-	10
Bu	740.3 (G1)	0	0	0	23	10^{-5}	Y	Y	30.6	.55	8.71	.11	27	2.61	13
Bu	740.3 (G1)	0	0	0	23	10^{-5}	Y	Y	29.0	.52	8.01	.16	27	2.61	13
Bu	740.3 (G1)	0	0	0	23	10^{-5}	Y	Y	29.2	.67	3.18	.13	27	2.61	18
Bu	740.3 (G1)	0	0	0	23	10^{-5}	Y	Y	26.4	.66	3.24	.13	27	2.61	18
Bu	740.3 (G1)	0	0	0	23	10^{-5}	Y	Y	23.6	.69	2.64	.13	27	2.61	18
Bu	747.3 (A1)	0	0	0	23	10^{-4}	R	Y	54	-	6.37	.05	20	-	10
Bu	752.2 (G1)	0	0	0	23	10^{-5}	Y	Y	36.6	-	-	-	28	2.60	13
Bu	752.2 (G1)	0	0	0	23	10^{-5}	Y	Y	46.3	.56	12.6	.14	28	2.60	13
Bu	752.2 (G1)	0	0	0	23	10^{-5}	Y	Y	37.2	.74	3.82	.12	28	2.60	18
Bu	752.2 (G1)	0	0	0	23	10^{-5}	Y	Y	45.2	.60	6.56	.12	28	2.60	18
Bu	757.8 (G1)	0	0	0	23	10^{-5}	Y	Y	38.3	.36	12.0	-	23	2.57	8
Bu	757.8 (G1)	0	0	0	23	10^{-5}	Y	Y	49.9	.40	15.8	-	23	2.57	8
Bu	757.8 (G1)	0	0	0	23	10^{-5}	Y	Y	60.1	.40	18.2	-	23	2.57	8
Bu	757.8 (G1)	0	0	0	23	10^{-5}	Y	Y	47	.52	13.7	.11	23	2.57	18
Bu	757.8 (G1)	0	0	0	23	10^{-5}	Y	Y	46	.51	13.1	.09	23	2.57	18
Bu	757.8 (G1)	0	0	0	23	10^{-5}	Y	Y	59	.58	14.6	.14	23	2.57	18

Appendix - Continued

Unit	Depth (m)	P_c (MPa)	P_p (MPa)	P_e (MPa)	T (°C)	$\dot{\epsilon}$ (s^{-1})	S (Y,R,N)	D (Y,N)	$(\Delta\sigma)_u$ (MPa)	$(\epsilon_1)_u$ (%)	E (GPa)	ν	~n (%)	~ ρ_g (Mg/m^3)	Ref
Bu	759 (G1)	5	0	5	200	10^{-4}	R	Y	87	-	16.5	-	27	2.61	9
Bu	759 (G1)	10	5	5	200	10^{-4}	Y	Y	70	-	13.1	-	27	2.61	9
Bu	759 (G1)	10	0	10	200	10^{-4}	R	Y	93	-	15.7	-	27	2.61	9
Bu	759 (G1)	17.5	5	12.5	200	10^{-4}	Y	Y	83	-	17.8	-	27	2.61	9
Bu	759 (G1)	20.7	0	20.7	200	10^{-4}	R	Y	119	-	17.6	-	27	2.61	9
Bu	759 (G1)	20.7	0	20.7	200	10^{-4}	R	Y	148	-	20.5	-	27	2.61	9
Bu	759 (G1)	24.1	3.4	20.7	200	10^{-4}	Y	Y	86	-	13.8	-	27	2.61	9
Bu	759.2 (A1)	20.7	0	20.7	23	10^{-4}	R	Y	140	-	22.1	.28	18	-	10
Bu	762.4 (G1)	0	0	0	23	10^{-5}	Y	Y	58.0	.41	15.1	-	24	2.61	8
Bu	762.4 (G1)	0	0	0	23	10^{-5}	Y	Y	72.9	.49	17.2	-	24	2.61	8
Bu	762.4 (G1)	0	0	0	23	10^{-5}	Y	Y	73.2	.40	20.8	-	24	2.61	8
Bu	762.4 (G1)	0	0	0	23	10^{-5}	Y	Y	59	.45	17.2	.14	24	2.61	18
Bu	762.4 (G1)	0	0	0	23	10^{-5}	Y	Y	59	.48	16.4	.11	24	2.61	18
Bu	762.4 (G1)	0	0	0	23	10^{-5}	Y	Y	58	.47	15.8	.13	24	2.61	18
Bu	773.5 (G1)	0	0	0	23	10^{-5}	Y	Y	117	.75	14.0	.09	24	2.58	18
Bu	781.2 (G1)	0	0	0	23	10^{-5}	Y	Y	120	.58	21.9	.14	21	2.47	13
Bu	781.2 (G1)	0	0	0	23	10^{-5}	Y	Y	153	.54	28.9	.14	21	2.47	13
Bu	781.2 (G1)	0	0	0	23	10^{-5}	Y	Y	101	.52	20.6	.12	21	2.47	18
Bu	781.2 (G1)	0	0	0	23	10^{-5}	Y	Y	104	.55	22.7	.19	21	2.47	18
Bu	787.9 (G1)	0	0	0	23	10^{-5}	Y	Y	71.7	.51	15.2	.08	24	2.39	13
Bu	787.9 (G1)	0	0	0	23	10^{-5}	Y	Y	83.7	.58	15.7	.12	24	2.39	13
Bu	787.9 (G1)	0	0	0	23	10^{-5}	Y	Y	73.9	.69	12.5	.13	24	2.39	18
Bu	787.9 (G1)	0	0	0	23	10^{-5}	Y	Y	67.1	.64	11.6	.17	24	2.39	18

Appendix - Continued

Unit	Depth (m)	P_c (MPa)	P_p (MPa)	P_e (MPa)	T (°C)	$\dot{\epsilon}$ (s^{-1})	S (Y,R,N)	D (Y,N)	$(\Delta\sigma)_u$ (MPa)	$(\epsilon_1)_u$ (%)	E (GPa)	ν	~n (%)	~ ρ_g (Mg/m^3)	Ref
Bu	794.9 (G1)	0	0	0	23	10^{-5}	Y	Y	71.9	.45	18.4	.14	24	2.47	13
Bu	794.9 (G1)	0	0	0	23	10^{-5}	Y	Y	73.5	.47	19.4	.13	24	2.47	13
Bu	794.9 (G1)	0	0	0	23	10^{-5}	Y	Y	60.4	.51	11.7	.10	24	2.47	18
Bu	794.9 (G1)	0	0	0	23	10^{-5}	Y	Y	72.7	.49	17.2	.16	24	2.47	18
Bu	804.9 (G1)	0	0	0	23	10^{-5}	Y	Y	50.2	.57	10.4	.14	28	2.49	13
Bu	804.9 (G1)	0	0	0	23	10^{-5}	Y	Y	45.2	.63	6.99	.12	28	2.49	18
Bu	804.9 (G1)	0	0	0	23	10^{-5}	Y	Y	47.0	.69	6.66	.11	28	2.49	18
Tr	822.7 (G1)	0	0	0	23	10^{-5}	Y	Y	60.1	.46	14.5	.16	33	2.52	14
Tr	822.7 (G1)	0	0	0	23	10^{-5}	Y	Y	53.6	.51	13.3	.18	33	2.52	14
Tr	822.7 (G1)	0	0	0	23	10^{-5}	Y	Y	45.3	.50	9.47	.11	33	2.52	18
Tr	822.7 (G1)	0	0	0	23	10^{-5}	Y	Y	63.9	.58	10.9	.11	33	2.52	18
Tr	856.5 (G1)	0	0	0	23	10^{-5}	Y	Y	42.0	.36	15.2	.38	23	2.61	14
Tr	856.5 (G1)	0	0	0	23	10^{-5}	Y	Y	46.0	.43	14.2	.31	23	2.61	14
Tr	856.5 (G1)	0	0	0	23	10^{-5}	Y	Y	76.2	.39	14.9	.17	23	2.61	18
Tr	856.5 (G1)	0	0	0	23	10^{-5}	Y	Y	66.4	.42	14.2	.21	23	2.61	18
Tr	883.0 (G1)	0	0	0	23	10^{-5}	Y	Y	68.1	.43	21.3	.27	21	2.62	14
Tr	883.0 (G1)	0	0	0	23	10^{-5}	Y	Y	69.2	.45	19.9	.24	21	2.62	14
Tr	883.0 (G1)	0	0	0	23	10^{-5}	Y	Y	95.8	.50	18.3	.27	21	2.62	18
Tr	883.0 (G1)	0	0	0	23	10^{-5}	Y	Y	115	.55	20.0	.22	21	2.62	18
Tr	913.4 (G1)	0	0	0	23	10^{-5}	Y	Y	67.6	.36	22.5	.23	21	2.59	14
Tr	913.4 (G1)	0	0	0	23	10^{-5}	Y	Y	40.9	.29	18.9	-	21	2.59	14
Tr	913.4 (G1)	0	0	0	23	10^{-5}	Y	Y	84.2	.63	10.1	.07	21	2.59	18
Tr	913.4 (G1)	0	0	0	23	10^{-5}	Y	Y	90.7	.39	21.8	.24	21	2.59	18

Appendix - Continued

Unit	Depth (m)	P_c (MPa)	P_p (MPa)	P_e (MPa)	T (°C)	$\dot{\epsilon}$ (s^{-1})	S (Y,R,N)	D (Y,N)	$(\Delta\sigma)_u$ (MPa)	$(\epsilon_1)_u$ (%)	E (GPa)	ν	~n (%)	~ ρ_g (Mg/m^3)	Ref
Tr	923.8 (G1)	0	0	0	23	10^{-5}	Y	Y	33.1	.37	13.4	-	26	2.58	14
Tr	923.8 (G1)	0	0	0	23	10^{-5}	Y	Y	28.6	.46	10.5	.28	26	2.58	14
Tr	923.8 (G1)	0	0	0	23	10^{-5}	Y	Y	51.7	.45	10.9	.14	26	2.58	18
Tr	923.8 (G1)	0	0	0	23	10^{-5}	Y	Y	64.7	.51	11.9	.21	26	2.58	18
Tr	945.6 (G1)	0	0	0	23	10^{-5}	Y	Y	20.2	.42	5.80	.20	33	2.56	14
Tr	945.6 (G1)	0	0	0	23	10^{-5}	Y	Y	41.5	.50	7.20	.14	33	2.56	14
Tr	945.6 (G1)	0	0	0	23	10^{-5}	Y	Y	37.1	.50	6.78	.16	33	2.56	18
Tr	975.4 (G1)	0	0	0	23	10^{-5}	Y	Y	33.0	.47	8.60	.17	26	2.61	14
Tr	975.4 (G1)	0	0	0	23	10^{-5}	Y	Y	25.8	.48	7.36	-	26	2.61	14
Tr	975.4 (G1)	0	0	0	23	10^{-5}	Y	Y	32.2	.78	2.61	.07	26	2.61	18
Tr	975.4 (G1)	0	0	0	23	10^{-5}	Y	Y	52.6	.55	7.92	.19	26	2.61	18
Tr	976.2 (G1)	0	0	0	23	10^{-2}	Y	Y	31.1	.52	6.63	-	25	2.61	14
Tr	976.2 (G1)	0	0	0	23	10^{-2}	Y	Y	24.4	.50	5.17	-	25	2.61	14
Tr	976.2 (G1)	0	0	0	23	10^{-4}	Y	Y	25.3	.50	6.42	-	25	2.61	14
Tr	976.2 (G1)	0	0	0	23	10^{-4}	Y	Y	22.1	.32	8.76	-	25	2.61	14
Tr	976.2 (G1)	0	0	0	23	10^{-4}	Y	Y	32.6	.44	8.97	.09	25	2.61	14
Tr	976.2 (G1)	0	0	0	23	10^{-6}	Y	Y	14.5	.31	7.04	.30	25	2.61	14
Tr	976.2 (G1)	0	0	0	23	10^{-6}	Y	Y	26.5	.50	8.26	.14	25	2.61	14
Tr	1008.3 (G1)	0	0	0	23	10^{-5}	Y	Y	25.6	.33	8.47	.26	33	2.64	14
Tr	1008.3 (G1)	0	0	0	23	10^{-5}	Y	Y	46.4	.51	9.39	.11	33	2.64	18
Tr	1008.3 (G1)	0	0	0	23	10^{-5}	Y	Y	51.7	.57	8.26	.11	33	2.64	18
Tr	1037.9 (G1)	0	0	0	23	10^{-5}	Y	Y	30.0	.35	8.85	.18	28	2.66	14
Tr	1037.9 (G1)	0	0	0	23	10^{-5}	Y	Y	37.3	.34	12.4	.31	28	2.66	14
Tr	1037.9 (G1)	0	0	0	23	10^{-5}	Y	Y	29.9	.39	6.66	.23	28	2.66	18
Tr	1037.9 (G1)	0	0	0	23	10^{-5}	Y	Y	41.2	.37	9.95	.29	28	2.66	18

Appendix - Continued

Unit	Depth (m)	P_c (MPa)	P_p (MPa)	P_e (MPa)	T (°C)	$\dot{\epsilon}$ (s^{-1})	S (Y,R,N)	D (Y,N)	$(\Delta\sigma)_u$ (MPa)	$(\epsilon_1)_u$ (%)	E (GPa)	ν	~n (%)	~ ρ_g (Mg/m^3)	Ref
Tr	1066.3 (G1)	0	0	0	23	10^{-5}	Y	Y	17.8	.34	5.56	.31	42	2.69	14
Tr	1066.3 (G1)	0	0	0	23	10^{-5}	Y	Y	17.4	.31	5.47	-	42	2.69	14
Tr	1066.3 (G1)	0	0	0	23	10^{-5}	Y	Y	27.6	.41	6.30	.17	42	2.69	18
Tr	1066.3 (G1)	0	0	0	23	10^{-5}	Y	Y	26.1	.46	4.90	.15	42	2.69	18

Distribution:

J. W. Bennett, Director
Geologic Repository Division
U. S. Department of Energy
S-10
Washington, D. C. 20545

M. W. Frei
Geologic Repository Division
U. S. Department of Energy
S-10
Washington, D. C. 20545

C. R. Cooley
Geologic Repository Division
U. S. Department of Energy
S-10
Washington, D. C. 20545

C. H. George
Geologic Repository Division
U. S. Department of Energy
S-10
Washington, D. C. 20545

J. J. Fiore
Geologic Repository Division
U. S. Department of Energy
S-10
Washington, D. C. 20545

J. G. Vlahakis
Geologic Repository Division
U. S. Department of Energy
S-10
Washington, D. C. 20545

T. P. Longo
Geologic Repository Division
U. S. Department of Energy
S-10
Washington, D. C. 20545

C. Klingsberg
Geologic Repository Division
U. S. Department of Energy
S-10
Washington, D. C. 20545

NTS Project Manager
High-Level Waste Technical Development Branch
Division of Waste Management
U. S. Nuclear Regulatory Commission
Washington, DC 20555

Chief, High-Level Waste Technical Development Branch
Division of Waste Management
U. S. Nuclear Regulatory Commission
Washington, DC 20555

J. O. Neff, Program Manager
National Waste Terminal Storage Program Office
U. S. Department of Energy
505 King Avenue
Columbus, OH 43201

N. E. Carter
Battelle
Office of Nuclear Waste Isolation
505 King Avenue
Columbus, OH 43201

ONWI Library (5)
Battelle
Office of Nuclear Waste Isolation
505 King Avenue
Columbus, OH 43201

O. L. Olson, Project Manager
Basalt Waste Isolation Project Office
U. S. Department of Energy
Richland Operations Office
P. O. Box 550
Richland, WA 99352

R. Deju
Rockwell International Atomics
Rockwell Hanford Operations
Richland, WA 99352

G. Tomsic
Utah Department of Community Economic Development
Room 6290, State Office Building
Salt Lake City, UT 89114

Governor's Office Planning Coordinator
Nevada State Planning Coordination
State Capitol Complex, Second Floor
Carson City, NV 89710

P. J. Iverson
Department of Minerals
State of Nevada
400 West King Street
Carson City, NV 89710

R. R. Loux, Jr.
c/o Department of Minerals
State of Nevada
400 West King Street
Carson City, NV 89710

K. Street, Jr.
Lawrence Livermore National Laboratory
Mail Stop L-209
P. O. Box 808
Livermore, CA 94550

L. D. Ramspott
Technical Project Officer
Lawrence Livermore National Laboratory
P. O. Box 808
Mail Stop L-204
Livermore, CA 94550

D. C. Hoffman
Los Alamos National Laboratory
P. O. Box 1663
Mail Stop E-515
Los Alamos, NM 87545

D. T. Oakley
Technical Project Officer
Los Alamos National Laboratory
P. O. Box 1663
Mail Stop F-671
Los Alamos, NM 87545

A. R. Hakl, Site Manager
Westinghouse - AESD
P. O. Box 708
Mail Stop 703
Mercury, NV 89023

P. L. Aamodt
Los Alamos National Laboratory
P. O. Box 14100
Las Vegas, NV 89114

D. L. Vieth, Director (6)
Waste Management Project Office
P. O. Box 14100
Las Vegas, NV 89114

D. F. Miller, Director
Office of Public Affairs
U. S. Department of Energy
P. O. Box 14100
Las Vegas, NV 89114

D. A. Nowack (11)
U. S. Department of Energy
P. O. Box 14100
Las Vegas, NV 89114

B. W. Church, Director
Health Physics Division
U. S. Department of Energy
P. O. Box 14100
Las Vegas, NV 89114

A. E. Gurrola
Holmes & Narver, Inc.
P. O. Box 14340
Las Vegas, NV 89114

W. W. Dudley, Jr.
Technical Project Officer
U. S. Geological Survey
P. O. Box 25046
Mail Stop 418
Federal Center
Denver, CO 80225

M. E. Spaeth (3)
Science Applications, Inc.
2769 South Highland Drive
Las Vegas, NV 89109

W. S. Twenhofel
820 Estes Street
Lakewood, CO 80215

H. D. Cunningham
Reynolds Electrical & Engineering Company, Inc.
P. O. Box 14400
Mail Stop 555
Las Vegas, NV 89114

J. A. Cross
Fenix & Scisson, Inc.
P. O. Box 15408
Las Vegas, NV 89114

R. H. Marks
U. S. Department of Energy
CP-1, MS 210
P. O. Box 14100
Las Vegas, NV 89114

Center for Tectonophysics
Texas A&M University
College Station, TX 77843

RE/SPEC, Inc. (2)
P. O. Box 725
Rapid City, SD 57701
Attn:
P. F. Gnirk
D. K. Parrish

1500	W. Herrmann
1510	D. B. Hayes
1520	T. B. Lane
1521	R. D. Krieg
1521	R. K. Thomas
1530	L. W. Davison
1534	J. R. Asay
1540	W. C. Luth
1541	H. C. Hardee
1542	B. M. Butcher
1542	L. S. Costin
1542	D. J. Holcomb
1542	W. A. Olsson
1542	R. H. Price (25)
1542	L. W. Teufel
1542	W. R. Wawersik
1542	D. H. Zeuch
1543	T. M. Gerlach
3141	L. J. Erickson (5)
3151	W. L. Garner (3)
3154-3	C. Dalin (25)
7417	F. L. McFarling
8214	M. A. Pound
6310	
6311	L. W. Scully
6312	L. D. Tyler
6312	J. K. Johnstone
6312	B. S. Langkopf
6312	R. R. Peters
6313	J. R. Tillerson (15)
6313	F. B. Nimick
6313	B. M. Schwartz
6313	R. M. Zimmerman
6314	
6314	J. L. Jackson
6314	A. E. Stephenson
6331	A. R. Lappin

Org.	Bldg.	Name	Rec'd by	Org.	Bldg.	Name	Rec'd by

Sandia National Laboratories